WILEY

Cladistics

Cladistics (2026) 1–25

doi: 10.1111/cla.70059

A new Cretaceous family illuminates the early evolutionary history of True Sawflies (Hymenoptera: Tenthredinoidea)

Jialiang Zhuang[a,b], Lars Vilhelmsen[c], Qi Feng[b], Corentin Jouault[d], Chungkun Shih[b,e], Dong Ren[b,*] and Mei Wang[a,*]

[a]*Key Laboratory of Biodiversity Conservation of National Forestry and Grassland Administration, Ecology and Nature Conservation Institute, Chinese Academy of Forestry, Beijing, China;* [b]*College of Life Sciences, Capital Normal University, Beijing, China;* [c]*Natural History Museum Denmark, SCIENCE, University of Copenhagen, Copenhagen, Denmark;* [d]*Oxford University Museum of Natural History, University of Oxford, Oxford, UK;* [e]*Department of Paleobiology, National Museum of Natural History, Smithsonian Institution, Washington, DC, USA*

Received 10 March 2026; Revised 24 June 2026; Accepted 16 July 2026

Abstract

A new family, †Eotenthredinidae, including two new species, †*Eotenthredo sinensis* gen. et sp. nov. and †*Eotenthredo magna* sp. nov., is described, based on nine adult specimens from the Early Cretaceous Yixian Formation, ~125 Ma. As the oldest known crown tenthredinoids to date, †Eotenthredinidae exhibits a mosaic of plesiomorphic and derived traits, serving as a crucial transitional taxon linking stem and crown tenthredinoids. We conduct a morphology-based phylogenetic analysis of Tenthredinoidea incorporating the most extensive sampling of Mesozoic fossils to date. Our results support the monophyly of Tenthredinoidea, recover the †'Xyelotomidae' as a paraphyletic grade and place †Eotenthredinidae as the sister group to core tenthredinoids. Morphometric analyses of the mesothorax further support the intermediate position of †Eotenthredinidae. Combining lineage-through-time analyses of plants and statistical analysis of tenthredinoid fossils, we emphasize the deep-time evolutionary association between tenthredinoids and their host plants. This study provides critical paleontological evidence for clarifying the early evolutionary history of Tenthredinoidea and deepens our understanding of plant–insect co-evolution and ecosystem restructuring during the Cretaceous Terrestrial Revolution from the insect perspective.

Introduction

The Cretaceous Terrestrial Revolution (KTR), a pivotal period of global ecosystem restructuring, is *inter alia* characterized by the rise of angiosperms and the adaptive radiation of insects that currently dominate terrestrial ecosystems (Benton et al., 2022; Wang et al., 2022; Ding et al., 2025). Since Darwin highlighted the 'abominable mystery' of angiosperm origins (Friedman, 2009), understanding how early pollinators and herbivorous insects responded to and facilitated the diversification of flowering plants has become a central question in palaeontology and evolutionary biology (Ren, 1998; Labandeira, 2014).

Among insects, the 'Symphyta' represent ancient herbivorous lineages within the Hymenoptera, and multiple lines of evidence suggest that these groups established complex ecological associations with diverse plants from as early as the Mesozoic (Krasilov and Rasnitsyn, 1982; Krassilov et al., 2003; Nyman et al., 2019; Xiao et al., 2024). Within these lineages, the Tenthredinoidea or true sawflies, today the most species-rich non-apocritan hymenopteran superfamily (>7000 extant species), originated during the Early Jurassic and form the cornerstone of this long-term plant-insect association (Taeger et al., 2018; Wutke et al., 2024; Jouault et al., 2025). Over their evolutionary history, Tenthredinoidea have undergone host shifts between ferns, gymnosperms and angiosperms,

*Corresponding author:
E-mail address: wangmei@caf.ac.cn (M.W.) rendong@mail.cnu.edu.cn (D.R.)

leaving abundant fossil evidence across multiple geological periods (Nyman et al., 2019). Nowadays, true sawfly larvae, in addition to the still predominant external feeding mode, have evolved diverse phytophagous feeding strategies such as leaf mining, gall induction, shoot and cone boring; furthermore, many groups engage in facultative pollination as adults (Jervis and Vilhelmsen, 2000; Nyman et al., 2006, 2019; Rodriguez et al., 2024). This combination of deep evolutionary roots and diverse feeding modes makes the Tenthredinoidea an ideal group for investigating insect responses to angiosperm radiation. Understanding the evolution of Tenthredinoidea and their roles in deep-time interactions with plants will help us to decode the establishment of modern-type terrestrial ecosystems during the KTR.

However, unravelling the co-evolutionary relationships between flowering plants and true sawflies requires robust evolutionary frameworks and improved resolution of long-standing phylogenetic uncertainties, particularly concerning early branching events and the groundplan states of crown-group lineages. Currently, nine families are recognized within Tenthredinoidea: Blasticotomidae, Pergidae, Argidae, Heptamelidae, Athaliidae, Cimbicidae, Diprionidae, Tenthredinidae and †Electrotomidae (established from fossil larvae only). Phylogenetically, the superfamily can be divided into a stem group, represented by extinct Mesozoic taxa historically placed in †'Xyelotomidae'—a group that was recently suggested to be synonymous with Blasticotomidae by Rasnitsyn and Müller (2023)—and a crown group comprising all remaining families (Rasnitsyn, 1969; Nel et al., 2004). Within the crown group, all families except Blasticotomidae constitute the core tenthredinoids or Tenthredinoidea *s. str.* (Ronquist et al., 1999). Although early morphology-based phylogenetic analyses distinguished the main tenthredinoid families, the high species diversity has proven an obstacle to obtaining resolution of deeper relationships within the superfamily (Vilhelmsen, 2001).

Recently, molecular advances have refined family-level classifications: Heptamelidae and Athaliidae have been separated from Tenthredinidae, and *Zenarge* Rohwer, 1918 (formerly within Argidae) was elevated to family rank, although this is disputed (Malm and Nyman, 2015; Malagón-Aldana et al., 2022; Niu et al., 2022; Wutke et al., 2024). However, these analyses focus predominantly on extant taxa, leaving extinct lineages—especially early diverging ones—unexplored.

To date, 27 Mesozoic tenthredinoid fossils have been reported (Table S1). They belong to 16 genera and show marked morphological divergence from extant groups. Most (25 of 27) used to be assigned to †'Xyelotomidae' (Sun et al., 2024). Rasnitsyn and Müller (2023) treated †'Xyelotomidae' as a synonym of Blasticotomidae based on similarities in larval and adult morphology, though without cladistic validation, so the association remains open to discussion. The other two species, †*Palaeathalia laiyangensis* Zhang, 1985 and †*Atefia rasnitsyni* Krogmann et al., 2012, may belong to the core group tenthredinoids owing to their thickened flagellomeres, but either lack diagnostic features or display unique character combinations, making it difficult place them more precisely among extant taxa (Zhang, 1985; Krogmann et al., 2012).

In contrast, more than 120 Cenozoic tenthredinoid species have been reported; no post-Mesozoic xyelotomids are recorded (Table S1). All Cenozoic fossils are crown tenthredinoids with small differences from extant taxa, and a considerable number are classified into extant genera (e.g. Vilhelmsen et al., 2024). Consequently, these fossils offer little information for early branching events and reconstructing crown-group groundplan states. Taken together, the current situation highlights a major gap in the evolutionary framework of tenthredinoids: namely, the ambiguous phylogenetic placement of stem lineages and early crown group due to the paucity of relevant material, and proper integration in a cladistic analysis of the existing fossils. This uncertainty further limits the utility of the fossils for calibrating divergence times and hinders our exploration of the early evolution of Tenthredinoidea.

Here, we report a new discovery from the Yixian Formation of the Jehol Biota: †Eotenthredinidae fam. nov., the oldest known crown-group Tenthredinoidea lineage to date, represented by two new species, †*Eotenthredo sinensis* gen. et sp. nov and †*Eotenthredo magna* sp. nov. These fossils provide critical information for a better understanding of early tenthredinoid evolution by combining clear synapomorphies with conserved plesiomorphic traits and thereby offer key evidence on the early evolution of tenthredinoids. To shed new light on tenthredinoid evolutionary trends and deepen our understanding of hymenopterans and insect evolution more broadly, we conducted a new morphology-based phylogenetic analysis of Tenthredinoidea incorporating extant and fossil lineages. Based on the phylogeny of Tenthredinoidea, we elucidate its deep phylogenetic framework and preliminarily assess the association between tenthredinoid lineage diversification and angiosperm radiation. Together, our work represents the most comprehensive integration of fossil and morphological evidence to date, offering valuable insights into plant–herbivore co-evolution and the restructuring of Cretaceous terrestrial ecosystems from a fossil perspective.

Materials and methods

Geological context, fossil provenance, examination of fossil and extant specimens

The new fossils (Fig. 1) were collected from the Early Cretaceous Yixian Formation. Specimens of †*Eotenthredo sinensis* originate from Huangbanjigou, Beipiao City, Liaoning Province, China; whereas †*E. magna* comes from Yangshuling, Pingquan City, Hebei Province, China (holotype) and Liutiaogou, Chifeng City, Inner Mongolia, China (paratype). Most of the fossil specimens used in this study are deposited in the Key Laboratory of Insect Evolution and Environmental Changes, College of Life Sciences, Capital Normal University, Beijing, China (CNUB; Dong Ren, Curator). Some of the extant specimens included in this study are deposited in the Natural History Museum of the Chinese Academy of Forestry (CAF), Beijing, China. For the remaining species, we examined high-resolution photographs from public data platforms (e.g. Global Biodiversity Information Facility [GBIF], Galerie du Monde des insectes) as well as from published articles. Detailed information regarding species names, sources and specimen numbers for both fossil and extant specimens is provided in Table S2.

Before imaging, matrix material obscuring the anatomical features was carefully removed to ensure full visibility of diagnostic characters in the fossil specimens. All specimens were examined and photographed using a Nikon SMZ 25 stereomicroscope equipped with a Nikon DS-Ri2 digital camera system, under dry conditions or wetted with 95% ethanol. Measurements of lengths and angles were obtained from high-resolution photographs using ImageJ2 software (Rueden et al., 2017). Wing venation terminology follows Rasnitsyn (1969, 1980), with minor modifications.

The Yixian Formation is an important source of information for the Jehol Biota and is internationally renowned for its exceptionally preserved Early Cretaceous fossils, including feathered dinosaurs, primitive birds, primitive mammals, the earliest known angiosperms, and exceptionally rich insect communities (Zhou et al., 2017; Ren et al., 2019). These fossils provide invaluable material for investigating major evolutionary questions such as the origin of angiosperms, and the co-evolution of organisms and their environment. The dating of the Yixian Formation has recently been refined to 125.755 ± 0.06–124.122 ± 0.048 Ma using U–Pb chemical abrasion-isotope dilution-isotope ratio mass spectrometry (CA-ID-IRMS; Zhong et al., 2021).

Exemplar taxa for phylogenetic analysis

We sampled 31 terminal taxa in total, comprising 19 extant taxa, 10 fossil taxa and two outgroups. This represents the most extensive sampling of Mesozoic tenthredinoid fossils to date. The 19 extant genera encompass all eight currently recognized extant families: Blasticotomidae, Pergidae, Argidae, Tenthredinidae, Heptamelidae, Athaliidae, Diprionidae and Cimbicidae; *Zenarge*, the family-level status of which remains debated, was also included. Among the fossil taxa, we included representatives of half the known genera

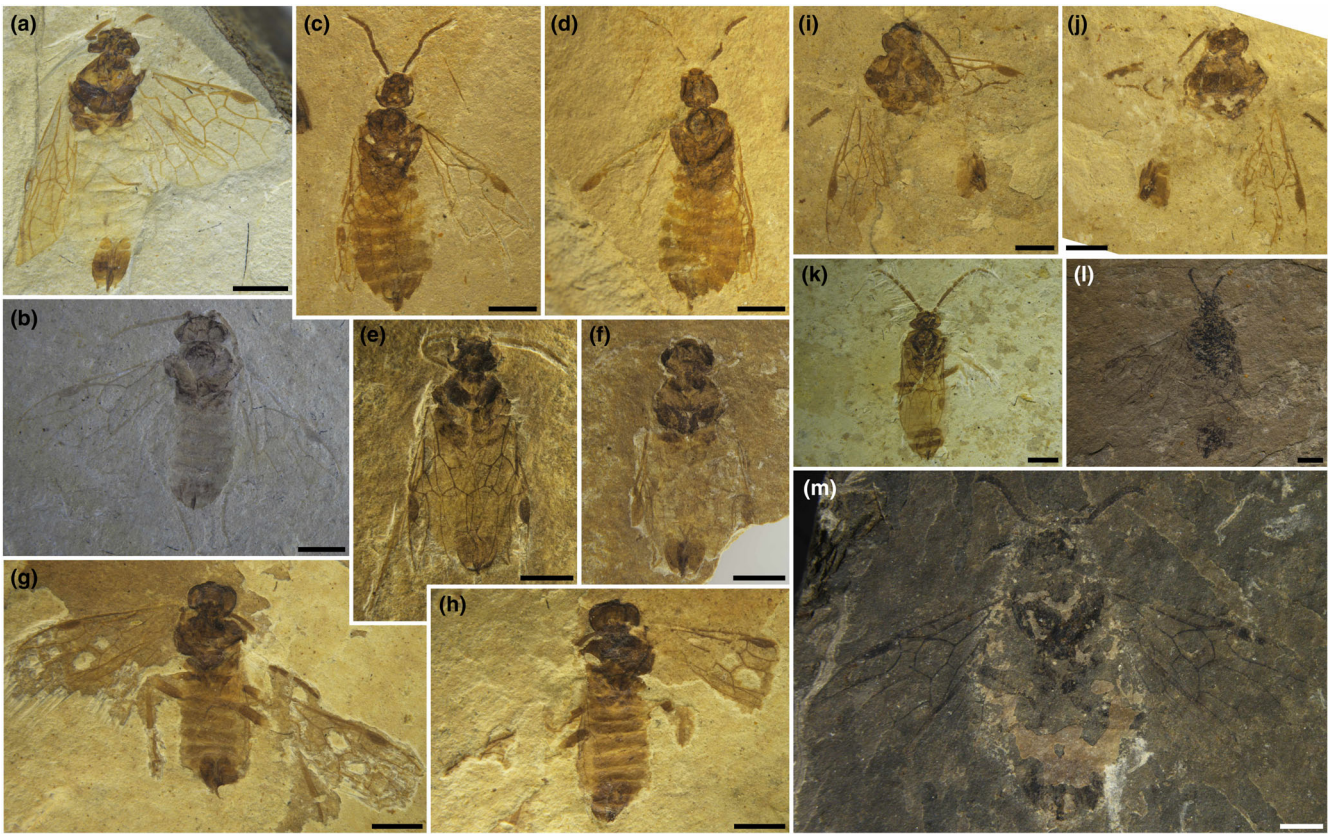

Fig. 1. Habitus images of †*Eotenthredo* gen. nov. spp. (a) †*Eotenthredo sinensis* sp. nov., holotype, CNU-HYM-LB2024001. (b–k) †*Eotenthredo sinensis* sp. nov., paratype, CNU-HYM-LB2024002-7. (l) †*Eotenthredo magna* sp. nov., paratype, CNU-HYM-NN2024009. (m) †*Eotenthredo magna* sp. nov., holotype, CNU-HYM-LB2024008. Scale bars: 2 mm in (a–m).

formerly assigned to †'Xyelotomidae' and the new genus †*Eotenthredo* (†Eotenthredinidae). When necessary, character states were combined from multiple paratypes to maximize scoring reliability and produce the most comprehensive morphological matrix possible.

Several Mesozoic taxa were excluded due to poor preservation, with only fore wings or heavily distorted bodies available. These include †*Xyelotoma* Rasnitsyn, 1968 (†'Xyelotomidae'), †*Abrotoma* Gao, Ren and Shih, 2009 (†'Xyelotomidae'), †*Pseudoxyela* Rasnitsyn, 1968 (†'Xyelotomidae'), †*Pseudoxyelocerus* Nel, Petrulevicius and Henrotay, 2004 (†'Xyelotomidae'), †*Undatoma* Rasnitsyn, 1977 (†'Xyelotomidae'), †*Aduantoma* Sun, Rasnitsyn, Zhuang and Shih, 2023 (†'Xyelotomidae'), †*Leridatoma* Rasnitsyn and Ansorge, 2000 (†'Xyelotomidae'), †*Atefia* Krogmann et al., 2012 (family *incertae sedis*) and †*Palaeathalia* Zhang, 1985 (family *incertae sedis*).

Most of the Cenozoic fossil taxa belong to extant families and show limited morphological differences with living representatives. Because these fossils contribute largely redundant and fragmentary morphological information, they were excluded from the cladistic analyses. Only some stratigraphically older and well-preserved Cenozoic specimens were incorporated into the analysis. †Electrotomidae were excluded, as they are known only from larval material (Rasnitsyn and Manukyan, 2023). Given that the adults are unknown, it cannot be excluded that this family is identical to one of the other more completely diagnosed tenthredinoid families. Furthermore, larval information is not available for any other fossil taxa.

Two herbivorous sawflies (Xyelidae and Pamphiliidae) were chosen as outgroups, due to their plesiomorphic antennae, wing venation, ovipositor and 'closer phylogenetic affinities' to Tenthredinoidea (Malm and Nyman, 2015; Wutke et al., 2024). The specific taxa selected were †*Evacuxyela* Dai, Shih and Rasnitsyn, 2022 and †*Scabolyda* Wang, Rasnitsyn, Shih and Ren, 2014.

Morphological dataset

The majority of morphological characters were derived from Vilhelmsen (2001, 2015). To better accommodate the determination of features in the impression fossils, we modified some characters and added some new characters (e.g. char 2, 5, 8, 10, 11, 14, 18, 23, 29, 31, 32, 37, 40) based on observations and taxonomic publications (see Data S1 for detailed references). The final matrix includes 31 genera (29 ingroup and two outgroup) and 61 characters (head: 1–6, thorax: 7–15, leg: 16–18, wing: 19–47, abdomen: 48–61, see Table 1). All multistate characters were treated as unordered. Unknown characters were coded as '?', and inapplicable characters were coded as '-'. The morphological character list is provided in Data S1, and some character states are illustrated in Figs 2–8 and Figs S1–S19.

Phylogenetic analysis

Unconstrained phylogenetic analyses were carried out using maximum parsimony (MP) and Bayesian inference (BI). Maximum parsimony analyses were conducted using TNT v.1.6 under both equal (EW) and implied (IW) weights (Goloboff and Catalano, 2016). Heuristic tree searches were run under the following parameters: tree bisection and reconnection (TBR) branch swapping algorithm, with 1000 replicates, saving 100 trees per replicate and keeping all trees found. For both EW and IW analyses, 10 times independent heuristic searches with zero random seed was run to find the best minimum length trees. Additionally, the K value was set to 12 in the IW analysis as recommended by Goloboff et al. (2018) and Zhang (2025). The MPTs were summarized by means of a strict consensus tree, and bootstrap (BS, using 1000 replicates) and relative Bremer support (BR) values were calculated under both EW and IW analyses. Character states were mapped on the tree using WinClada v.1.61 (Nixon, 2002), showing unambiguous changes. Consistency indices (CI) and retention indices (RI) were calculated using the '*Stats.run*' script in TNT.

Unconstrained BI analyses were carried out using MrBayes version v.3.2.7 (Ronquist et al., 2012). †*Evacuxyela* and †*Scabolyda* were set as the outgroups. An Mkv model with gamma rate distribution was set to analyse the morphological data (Lewis, 2001). Only variable characters were coded, and non-applicable morphological characters were treated as missing data. All multistate characters were treated as unordered, with equal transition probabilities between states and allowing for rate variation among characters. Two runs of four chains, three of which were heated, were run for a total of 2 500 000 generations, with sampling every 500 generations and the first 25% discarded as burn-in. The NEXUS file, including MrBayes commands, is provided in Data S1.

Given that the phylogenetic placements of Heptamelidae and Athaliidae are primarily based on molecular data and characters based on the arrangement of protein coding genes (Malm and Nyman, 2015; Niu et al., 2022), they are difficult to place using morphological characters alone (Vilhelmsen, 2015). This uncertainty directly affects the stability of the morphological tree topology and, most critically, obscures the phylogenetic placement of our new family. To further evaluate the position of †Eotenthredinidae within a robust molecular framework, we conducted a constrained phylogenetic analysis using the '*PlaceMyFossils*' script (Catalano et al., 2025) in TNT v.1.6. The reference tree, viz. molecular backbone tree (Fig. S20), used for constrained analysis was adopted from the molecular phylogeny of Wutke et al. (2024), in which all extant taxa, especially representatives of Heptamelidae and Athaliidae, were fixed according to their molecular phylogeny. Additionally, the backbone tree included not only extant taxa but also the two outgroup fossil taxa, †*Evacuxyela* (Xyelidae) and †*Scabolyda* (Pamphiliidae), the positions of which were fixed based on familial affinities. Next, †*Eotenthredo* gen. nov. was designated as the target species, and the remaining fossil taxa were treated as additional query species. Standard maximum parsimony optimality criteria and the same morphological character matrix from the unconstrained analysis were used to evaluate the placement of new fossil family. All other settings were kept at default values.

All results above are shown in Figs 9 and 10 and Figs S21 and S22.

Morphometric analysis of the mesothorax

In sawflies, the mesonotum (Fig. 11) is composed of two main parts, the mesoscutum and the mesoscutellum, and the latter is usually separated from the former by the scutoscutellar furrow. The mesoscutum is further divided by the converging notauli to form the triangular prescutum. The prescutum, mesoscutellum and the interval between them exhibit considerable morphological diversity among sawfly groups. Particularly, the length ratio of the prescutum relative to the mesothorax holds significant taxonomic value: in core tenthredinoids, this ratio typically reaches 1:2 (Richards, 1985); whereas in stem tenthredinoids, Blasticotomidae, Xyelidae and Pamphiliidae, the ratio is notably lower. Quantifying these morphological traits is important for understanding morphological variation within and evolutionary relationships among sawflies. Therefore, we selected the lengths of three thoracic structures—mesoprescutum (psc), mesoscutellum (scl) and the distance between them (gap)—and calculated their ratios relative to mesonotum (mn) length as key morphological characters to analyse variation patterns in the sawflies.

As shown in Fig. 11, psc was measured along the midline from its anterior margin to the posteriormost ending point; scl was measured medially from its anterior to posterior margins; and the gap was measured as the shortest distance between the posterior margin/point of the prescutum and the anterior margin of the scutellum. The postscutellum/mesoscutellar appendage (pscl, Fig. 11) is developed in Blasticotomidae, Athaliidae, Heptamelidae and most

Table 1
Distribution of character states. ? = not known/uncertain; - = not applicable; P = 0 & 1 (polymorphism)

Character	0000000001 1234567890	1111111112 1234567890	2222222223 1234567890	3333333334 1234567890	4444444445 1234567890	5555555556 1234567890	6 1
Evacuxyela	0–000p0000	0000??0000	0000000000	0003000000	000?000000	0?????????	?
Scabolyda	0–01000000	0001?10000	p000101100	1003000000	000000001?	1???????0?	?
Dahurotoma	0–00010000	00?1????00	1110110001	−103000010	000??0000?	1?????????	?
Aethotoma	0–00010000	0001?10000	1010110000	1103000010	000000000?	1?????????	?
Apertoma	0–00010000	0001?10000	1110110000	1103000010	000000000?	1???????0?	?
Paradoxotoma	0–00010000	0001??0000	1010110000	1003000010	0000?00?0?	1?????????	?
Synaptotoma	0–00010000	00??????00	1110110001	−103000010	000?000?0?	1?????????	?
Liberitoma	0–00010000	0001??0000	1010110000	1103000010	000000000?	1???????0?	?
Xyelocerus	0–00010000	0001??0000	111011p100	1103000010	000000000?	1?????????	?
Blasticotoma	0–00011001	1101011–1–	––10110110	1100000010	0000100001	10?0?01?0?	?
Eotenthredo	0–01001101	0000????01	––10111111	−103000010	000?10000?	1?????????	?
Zenarge	0–3–––1001	1001110101	––10111111	−1030001–0	0000111100	11–000111?	?
Arge	0–3–––1001	1011100101	––10111111	−1031001–1	01–1100000	11–1001110	1
Sterictiphora	0–3–––1001	1011101–1–	––10111111	−1031001–1	01–1100100	11–1001110	1
Acordulecera	0–21001001	111110011–	––10111111	−1000011––	12–1111100	11–1000100	1
Aulacomerus	0–11001001	1011?01–01	––10111111	−1030011––	02–?111100	11–???0???	?
Baladi	0–2100???1	????????01	––10111111	−1030011––	12–?111?0?	1?????????	?
Abia	2111001001	1111001–1–	––10111111	−1000p1011	11–1100102	1010111001	0
Cimbex	2111001001	1111001–1–	––10111111	−100011011	1011100102	1010?11000	0
Corynis	2011001001	1111001–1–	––10111111	−100001011	11–1100102	1010111001	0
Monoctenus	1–11001111	1111001–01	––10111111	−1010001–1	01–0100000	1000111001	0
Eodiprion	1–11001101	1111?01–01	––10111111	−1010001–1	01–?1????0	1?????????	?
Diprion	1–11001101	1111001–01	––10111111	−1010001–1	0011100000	1000111001	0
Heptamelus	0–11001011	1101001–1–	––10111––1	−102000011	1000100000	100010????	?
Athalia	0–11001011	1101001–1–	––10111111	−103000011	1000100000	1000111000	0
Nematinus	0–21101111	1101011–01	––10111111	−1030001–1	01–0100000	1000101000	0
Selandria	0–21101111	1101011–01	––10111111	−113000011	01–0100000	1000101000	0
Strongylogaster	0–21101111	1101011–01	––10111111	−113000011	01–0100000	1000101000	0
Taxonus	0–21101111	1101011–01	––10111111	−103011011	000p1p0000	100011????	?
Siobla	0–11101111	1101011–01	––11111111	−103010011	1000100000	10001?????	?
Tenthredo	0–21101111	1101011–01	––11111111	−10301p011	p010100000	1000111000	0

Tenthredinidae, but is typically lacking or reduced in other tenthredinoid families. Consequently, we exclude the postscutellum when measuring the length of the mesonotum.

Based on the ratios of these three parts (Table S3), a ternary diagram and violin plots for each part were constructed using Origin 2025 v.10.2.0, to visualize the data distribution. The mesothorax of the fossil specimen used for these measurements is illustrated in Figs 7 and 8 and Figs S2–S19. Measurements of other taxa are from high-resolution images, with image sources provided in Table S2.

Ancestral state reconstruction and heatmap

Ancestral state reconstructions were conducted in R v.4.3.3 (R Core Team, 2023) (Data S2). We focused on the relative length of the first flagellomere (Char. 3, length ratio of the first flagellomere to the second flagellomere), a key trait that varies across symphytan lineages and provides insights into their evolutionary patterns. This character was reconstructed to clarify its evolutionary trajectory. Analyses were based on the MP tree from morphological phylogenetic results (Fig. 10).

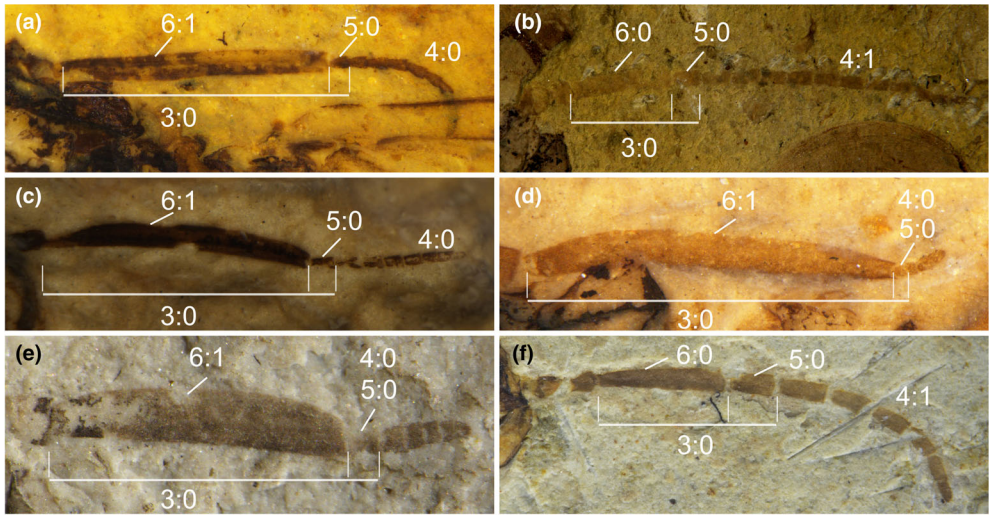

Fig. 2. Antennal anatomy variation in Mesozoic sawflies. (a) †*Evacuxyela hsiaoae*, male. (b) †*Scabolyda latusa*, female. (c) †*Liberitoma* sp., female. (d) †*Paradoxotoma tsaiae*., male. (e) †*Xyelocerus* sp., gender unknown. (f) †*Eotenthredo sinensis* sp. nov., female. Numbers refer to character states (see Data S1).

The phylogenetic tree and trait data were imported and matched via the '*ape*' and '*picante*' packages (Kembel et al., 2010; Paradis and Schliep, 2019). Discrete character evolution was modelled using an equal-rates model implemented via the '*fitDiscrete*' function in the '*geiger*' package v2.0.11 (Harmon et al., 2008). Reconstructed character states for tips and nodes were visualized on the tree using '*ape*' and '*phytools*' packages (Revell, 2024).

Given the absence of the second flagellomere in Argidae, we conducted a complementary morphometric analysis to characterize the proportional variation of the first flagellomere in more detail. Five ratios were evaluated (Table S4): (1) the length of the first flagellomere compared to that of the second (L_{fla1}/L_{fla2}), (2) the length of the first flagellomere compared to that of the thread (L_{fla1}/L_{thread}, thread = flagellomeres except the first one), (3) the length of the first flagellomere compared to width of the head (L_{fla1}/W_{head}), (4) the aspect ratio of the first flagellomere (L_{fla1}/W_{fla1}) and (5) the aspect ratio of the second flagellomere (L_{fla2}/W_{fla2}). Following standardization, the results were plotted as heat maps and added next to the corresponding terminals of the phylogenetic tree following the procedure detailed in Data S2.

Lineages-through-time (LTT) plots

Lineages-through-time plots were generated to compare diversity dynamics between plants and tenthredinoids. LTT plots for angiosperms, gymnosperms and ferns were modelled using PyRate (Silvestro et al., 2019) and created using the '*-ltt 1*' option to summarize diversification analyses based on fossil data (collected from PBDB database https://paleobiodb.org/) and phylogenetic analyses (Lehtonen et al., 2017; Feng et al., 2025). More details and scripts are in Data S2.

Due to the relatively sparse fossil record of Tenthredinoidea, which is insufficient for robust PyRate modelling, we adopted a different visualization approach. For tenthredinoids, the fossil species counts and compositions of Tenthredinoidea across different geological periods were added to the time scale in the form of histograms and a ten-grid chart, respectively. The 10 cells correspond precisely to all families within the crown tenthredinoids. It includes both extinct and extant families of crown tenthredinoids, specifically including †Eotenthredinidae but excluding 'Zenargidae'. For a detailed fossil list of Tenthredinoidea, see Table S1.

Results

Systematic palaeontology

Order Hymenoptera Linnaeus, 1758
Suborder 'Symphyta' Gerstaecker, 1867
Superfamily Tenthredinoidea Latreille, 1803

Family †Eotenthredinidae Zhuang, Wang, Vilhelmsen and Ren, fam. nov.

Diagnosis. Antenna filiform, 10–11 segmented and each segment of equal width; first flagellomere ca. 3× as long as second; following three flagellomeres similar in length and with aspect ratio less than three. Mesothorax with prescutum of more than half length of mesothorax; mesoscutellum triangular, mesoscutellar appendage absent; mesospseudosternal sulci present, meeting in midline and before anterior margin of the mesopleuron. Ovipositor short and slightly extending from abdomen. Fore wing with costal area developed, Sc only developed as crossvein and merging into R distal to M + Cu fork; pterostigma developed and sclerotized, with anterior margin straight and posterior margin strongly curved; 1-M and Rs + M converging at the bend of R; 1-Rs absent and 2-Rs present; cell 1mcu nearly quadrangular; 1r-rs perpendicular to the anterior margin of fore wing and its length slightly shorter than Rs + M; 2r-rs oblique and entering cell 3rm; 2 m-cu distal to 2r-m or connected with 2r-m; 2A + 3A developed, incurved and not fused with 1A. Hind wing with 3r-m, m-cu and cell a present.

Remarks. The new family †Eotenthredinidae can be distinguished from †'Xyelotomidae' and Blasticotomidae by all flagellomeres having approx. the same width, the mesoprescutum longer than half the length of the

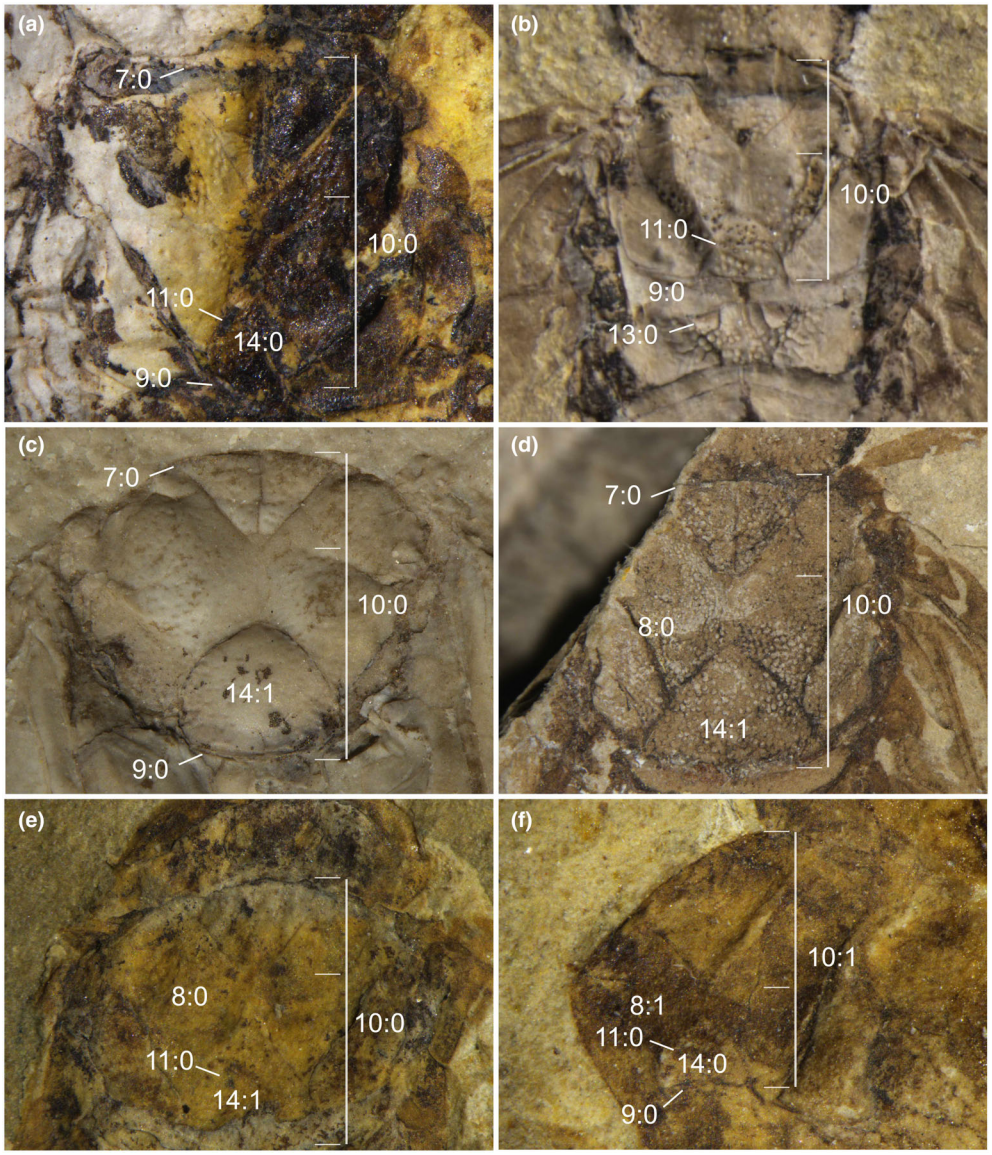

Fig. 3. Mesothorax anatomy variation in Mesozoic sawflies. (a) †*Evacuxyela hsiaoae*. (b) †*Scabolyda orientalis*. (c) †*Apertoma macroclada*. (d) †*Xyelocerus* sp. (e) †*Dahurotoma* sp. (f) †*Eotenthredo sinensis* sp. nov. Numbers refer to character states (see Data S1).

mesothorax, fore wing with Sc only developed as a crossvein, and 1-Rs absent. However, it still retains some plesiomorphic characteristics, for example, the antenna with the first flagellomere nearly three times as long as the second, mesoscutellum triangular (small and narrow), and left and right scutoscutellar sulcus meeting in an acute angle (<90°). These significant features were not previously observed in crown tenthredinoids. Furthermore, other unique combinations of features different from other crown tenthredinoids are listed below:

- 'Antenna straight with 10–11 segments; aspect ratio of each flagellomere less than three except for the first flagellomere'; similar antennal type and number of flagellomeres are currently only found in some tenthredinoids such as *Decameria* Lepeletier de Saint Fargeau and Audinet-Serville, 1828 (Pergidae), *Athalia* Leach, 1817 (Athaliidae) and *Heterarthrus* Stephens, 1835 (Tenthredinidae).
- 'Mesothorax with mesopseudosternal sulci present': only developed in most genera of Argidae, Pergidae and *Zenarge*. In these taxa, the sulci reach the anterior margin of the mesopleuron before merging medially. However, this differs from †Eotenthredinidae, in which they meet before reaching the anterior margin. The condition in †Eotenthredinidae is likely plesiomorphic and is observed among extant Hymenoptera only in Xyeloidea.

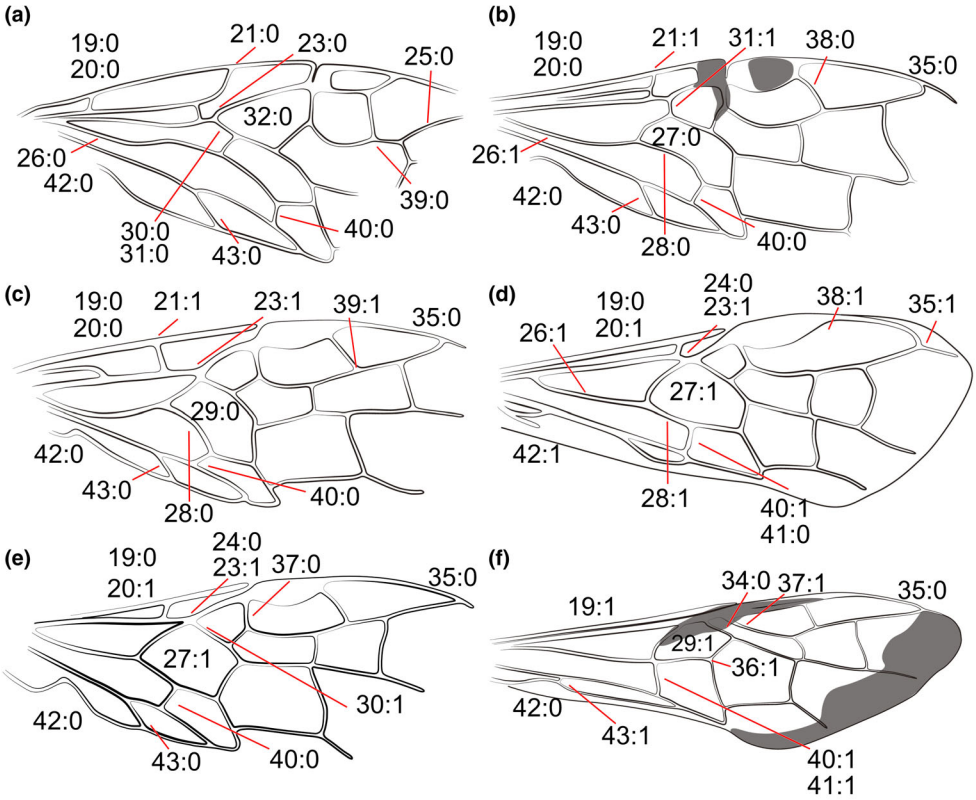

Fig. 4. Fore wing venation variation in Mesozoic and extant sawflies. (a) †*Evacuxyela hsiaoae*. (b) †*Liberitoma* sp. (c) †*Dahurotoma* sp. (d) *Arge nigripes*. (e) †*Eotenthredo sinensis* sp. nov. (f) *Cimbex femoratus*. Numbers refer to character states (see Data S1).

- 'Fore wing with Sc, 2-Rs and 2r-rs present': only Tenthredinidae possessed all these veins; other lineages exhibited varying degrees of loss; vein Sc is absent in Athaliidae, Heptamelidae, Cimbicidae, partly in Pergidae and Argidae; vein 2-Rs is reduced in Heptamelidae, Cimbicidae, Diprionidae and a few genera in other crown Tenthredinoidea; vein 2r-rs is absent in Diprionidae, Pergidae, Argidae, and *Zenarge*.
- 'Fore wing with anal vein complete like in xyelids': the structure of the anal veins is conspicuously modified (e.g. proximal part of vein 3A absent) in most Tenthredinoidea families except Athaliidae, Heptamelidae and some Tenthredinidae.
- 'Hind wing with m-cu and cell a present': absent mainly in Pergidae.

Based on the isolated phylogenetic position as well as the unique character combination, a case is made for erecting a new family.

Genus †Eotenthredo Zhuang, Wang, Vilhelmsen and Ren, gen. nov.

Diagnosis. As for family.

Etymology. The generic name is a combination of the Greek 'Eos' meaning early, and 'tenthredo', a combining form derived from the Greek 'tenthredōn' (a kind of wasp) and widely used in the names of sawflies. Gender: feminine.

Type species. †*Eotenthredo sinensis* Zhuang, Wang, Vilhelmsen and Ren, sp. nov.

Included species. Type species, †*E. sinensis* Zhuang, Wang, Vilhelmsen and Ren, sp. nov.; †*E. magna* Zhuang, Wang, Vilhelmsen and Ren, sp. nov. and †*E. rudgwickensis* Rasnitsyn and Jarzembowski, 1998 comb. nov. [= †*Undatoma rudgwickensis* Rasnitsyn and Jarzembowski, 1998, = †*Leridatoma rudgwickensis* (Rasnitsyn et al., 1998)].

†Eotenthredo sinensis Zhuang, Wang, Vilhelmsen and Ren, sp. nov.
(Fig. 5, Figs S1–S6)

Material. Holotype, CNU-HYM-LB2024001, deposited in CNUB. Paratypes, CNU-HYM-LB2024002 (CNUB); CNU-HYM-LB2024003p/c (part and counterpart; CNUB); CNU-HYM-LB2024004p/c (CNUB); CNU-HYM-LB2024005p/c (CNUB); CNU-HYM-LB2024006p/c (CNUB); CNU-HYM-LB2024007 (CNUB).

Diagnosis. In addition to the generic diagnosis, †*E. sinensis* is further characterized by the following features: the aspect ratio of the second flagellomere ca. 2×; fore wing with vein Rs + M longer than 2-Rs and

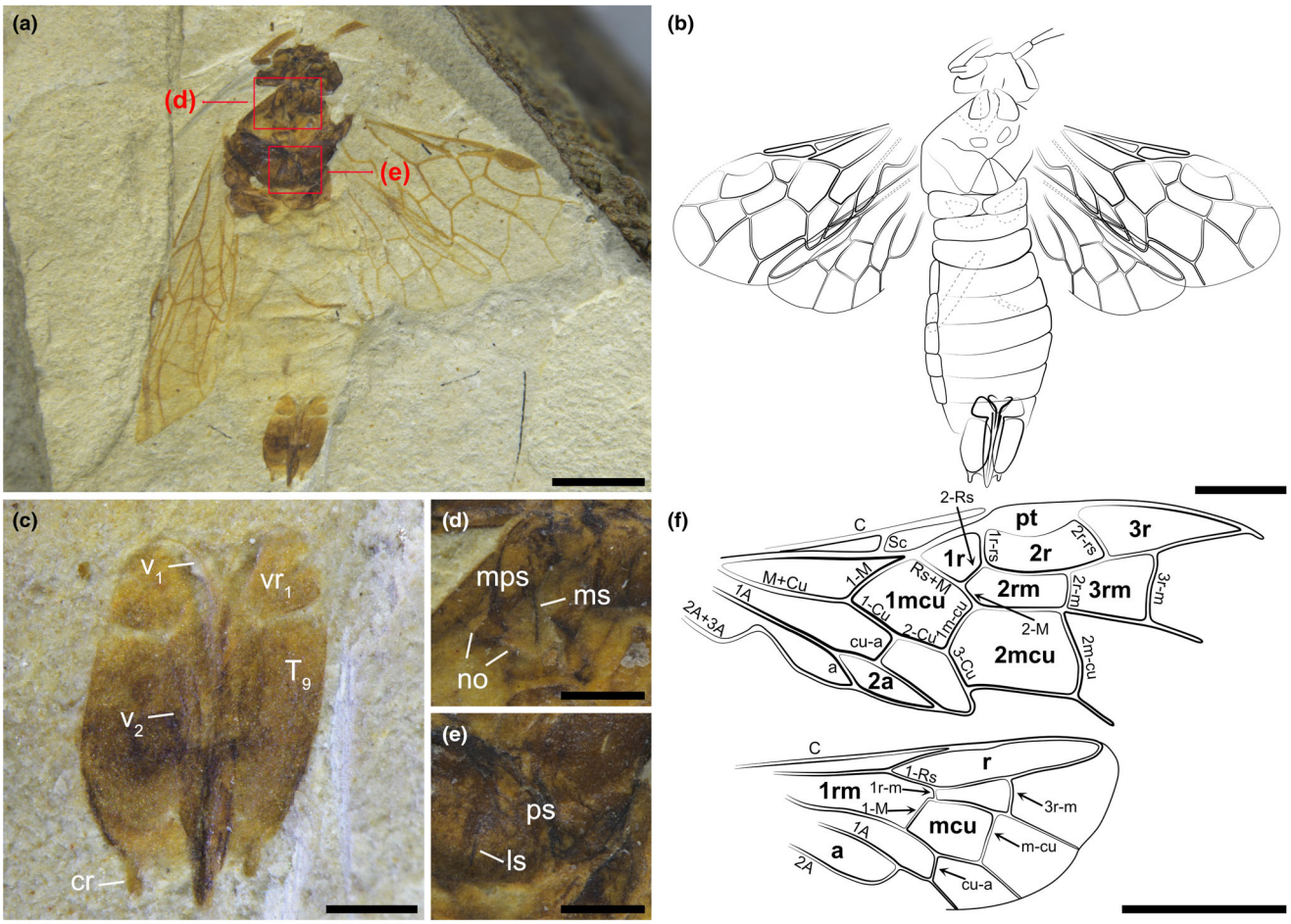

Fig. 5. †*Eotenthredo sinensis* sp. nov., holotype, CNU-HYM-LB2024001, female. (a) habitus, ventral view. (b) line drawing of ventral view. (c) ovipositor. (d) mesoprescutum. (e) mesopleuron, ventral view. (f) line drawing of fore wing and hind wing. Scale bars: 2 mm in (a, b, f); 0.5 mm in (c–e). cr, cercus; ls, lateral sulcus; mps, mesoprescutum; ms, mesal mesoscutal sulcus; no, notaulus; ps, pseudosternum; T_9, 9th tergum; v_1, v_2, 1st and 2nd valvula; vr_1, 1st valvifer.

ratio near 1.5× to 2×; vein 1r-rs far longer than half length of 2r-rs, and vein 2r-m posteriorly intersecting 2 m-cu.

Etymology. The species name is derived from the Latin word 'sinensis', meaning Chinese, referring to the geographical origin of the type specimens.

Locality and horizon. Huangbanjigou, Beipiao City, Liaoning Province, China. Yixian Formation, Lower Cretaceous.

Description. Holotype. CNU-HYM-LB2024001 (Fig. 5): Female. Body length 9.6 mm, head 1.0 mm in length and 1.9 mm in width, wider than long, flat and oval (Fig. 5b). Eyes large and reniform, occupying most of head lateral surface. Antenna with length of first flagellomere at least half width of head.

Thorax smooth without any punctation. Mesoprescutum triangular, its anterior margin strongly curved, median mesoscutal sulcus nearly reaching the posterior end of notaulus (Fig. 5d); mesopseudosternal sulci present (Fig. 5e).

Fore wing (Fig. 5f) 5.6 mm in length, 2.8 mm in width. Pterostigma wide, completely sclerotized and nearly 2.6× as long as wide, its posterior border markedly arched. Sc sub-perpendicular to vein R, entering R proximal to origin of Rs at a distance about half length of Rs + M. R not deviating between junctions of M and Sc; 1-Rs absent; 1r-rs and 2r-rs developed and latter inclined towards wing apex; 2r-m located at two thirds of cell 2r. Cell 3rm shorter than 2rm and noticeably widened at the ends. M + Cu slightly curved and branching before level of Sc; angle between 1-M and 1-Cu nearly 70°. 1-M nearly as long as 1-Cu; Rs + M nearly 1.6 times as long as 1r-rs; 2-M nearly half of Rs + M. 2-Cu meeting 1 m-cu at an angle of 112°. Cell 1mcu 1.3 times as long as wide (line connecting midpoint of 1-M and that of 1 m-cu:

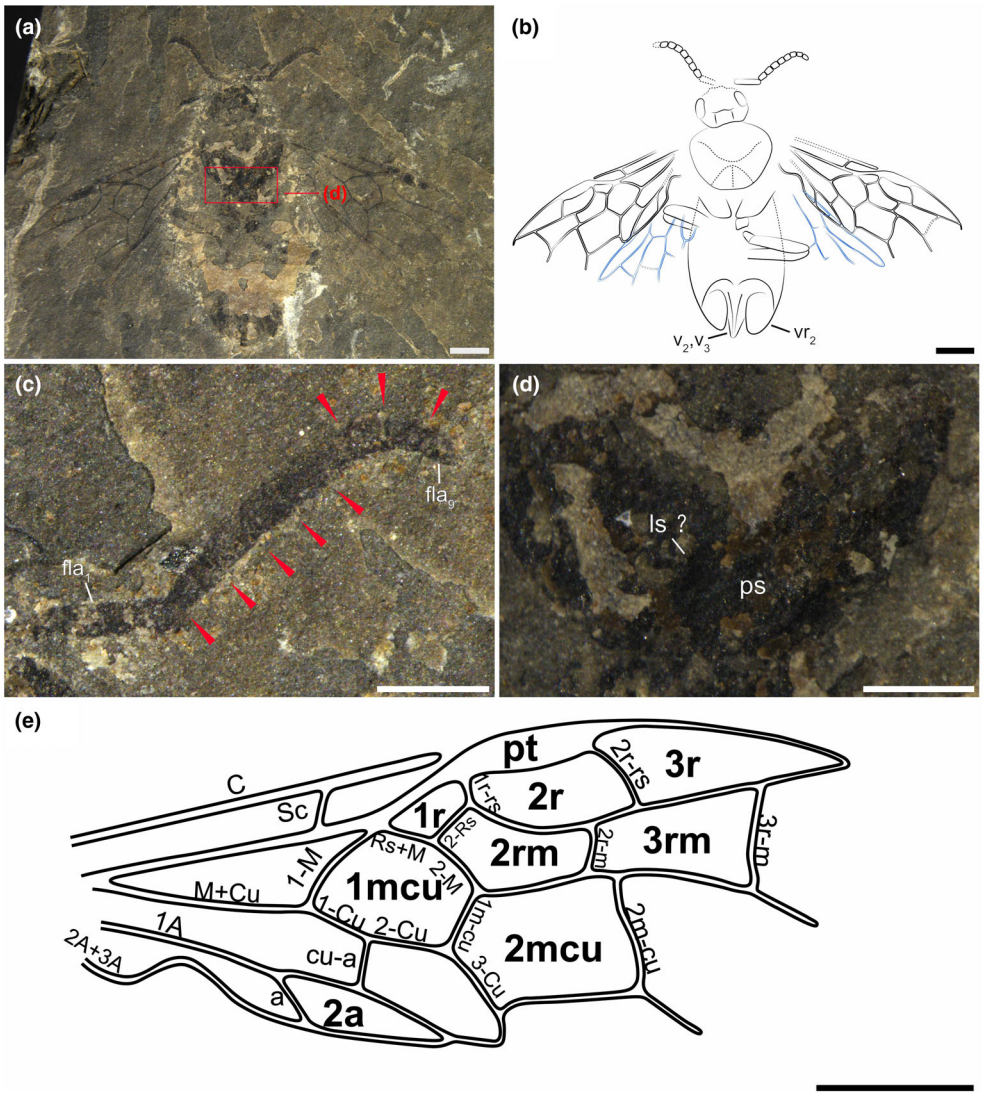

Fig. 6. †*Eotenthredo magna* sp. nov., holotype, CNU-HYM-LB2024008, female. (a) ventral view. (b) line drawing of ventral view. (c) antennae. (d) pseudosternum. (e) line drawing of fore wing. Red triangles mark the segmented parts of the flagellomeres. Scale bars: 2 mm in (a, b, e); 0.5 mm in (c, d). fla_1, fla_9, 1st and 9th flagellomere; v_3, 3rd valvula.

maximum distance perpendicular to line), approx. rectangular and 1-M sub-parallel to 1 m-cu. 3-Cu and 1 m-cu of similar length; cu-a perpendicular to vein A and located near middle of cell 1mcu. Posterior end of 2r-m almost connecting to anterior end of 2 m-cu. Cell 2a almost four times as long as wide.

Hind wing (Fig. 5f) 4.2 mm in length. Sc not developed. 1-Rs ca. 1.1× as long as 1-M; 1r-m located distal to base of 1-Rs and sub-perpendicular to vein C. 3r-m ca. 0.7× as long as m-cu and parallel to 1r-m; m-cu straight, located distal to middle of cell rm and separated from 3r-m by a distance of 1r-m length; cu-a located at middle of cell mcu and meeting 1-Cu at an angle of 116°. 1A slightly curved and cell a blunt apically.

Abdomen with nine segments preserved; cercus short and not reaching end of ovipositor in holotype. Ovipositor (Fig. 5c) 2.0 mm in length, gladiate and extending shortly beyond abdomen short; 1st valvulae separated basally.

Paratype. CNU-HYM-LB2024002 (Fig. S1): Female. Body length 8.4 mm. Head (Fig. S1b) flat, 1.2 mm in length and 2.4 mm in width, eyes large and longer than half length of head, postocellar furrows subparallel, antenna 4.0 mm with scape apparently wider than pedicel, the first flagellomere ca. 1.9 mm.

Thorax wider than head, mesothorax with mesopseudosternal sulci well developed (Fig. S1c).

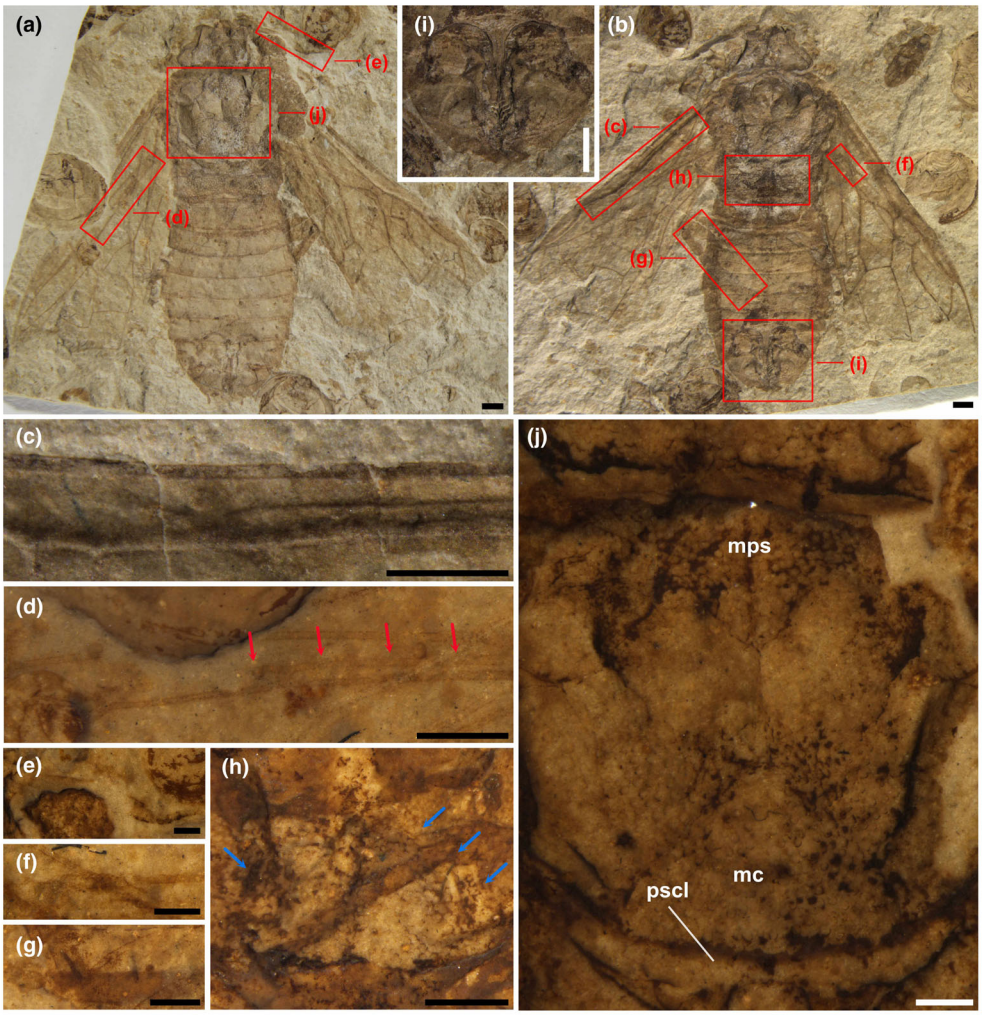

Fig. 7. †*Xyelocerus diaphanus* (CNU-HYM-NN2008011), female. (a) habitus, dorsal view. (b) habitus, ventral view. (c) Sc in fore wing. (d) Sc in hind wing under alcohol. (e) antennae under alcohol. (f) hamuli under alcohol. (g) hind leg with spurs under alcohol. (h) medioventral mesopleuron under alcohol. (i) ovipositor. (j) mesothorax under alcohol. Red arrows mark vein Sc in hind wing; blue arrows point to the possible pseudosternal sulci. Scale bars: 1 mm in (a–d, g–i); 0.5 mm in (e, f, j). mc, mesoscutellum; mps, mesoprescutum; pscl, postscutellum (= mesoscutellar appendage).

Fore wing 6.7 mm in length and 2.8 mm in width. Pterostigma wide, completely sclerotized and nearly 2.5× as long as wide. Cell 1mcu nearly rectangular, 1-M meeting 1-Cu at an angle of 74°, 1-Cu and 2-Cu arranged in straight line; posterior end of 2r-m connected to anterior of 2 m-cu, cell 2a approx. 3.7× as long as wide.

Paratype. CNU-HYM-LB2024003p/c (Fig. S2): Female. Body length 10.1 mm. Head (Fig. S2c) nearly round, 1.4 mm in length and 1.6 mm in width, eyes large and three ocelli arranged in a triangle. Antenna (Fig. S2d) 3.2 mm in length and 10-segmented, first flagellomere 1.2 mm in length and nearly four times as long as that of the second, thread 1.9 mm in length.

Thorax (Fig. S2f) wider than head, mesothorax with prescutum occupying nearly half length, median mesoscutal sulcus developed and nearly reaching posterior end of notaulus. Mesoscutellum small and both its width and length nearly half length of prescutum.

Fore wing 6.4 mm in length and 2.8 mm in width. Sc sub-perpendicular to vein R. 1-M meeting 1-Cu at an angle of 68.2°.

Abdomen with ovipositor short and slightly exposed at end of abdomen.

Paratype. CNU-HYM-LB2024004p/c (Fig. S3): Female. Body length 9.0 mm. Head (Fig. 3c) flat and oval, 1.2 mm in length and 2.1 mm in width. Antenna (Fig. 3g) with 10 segments, with first flagellomere 1.0 mm long and nearly half length of thread.

Thorax with each propleural sclerite reniform, anteriorly close to each other and posterior separated;

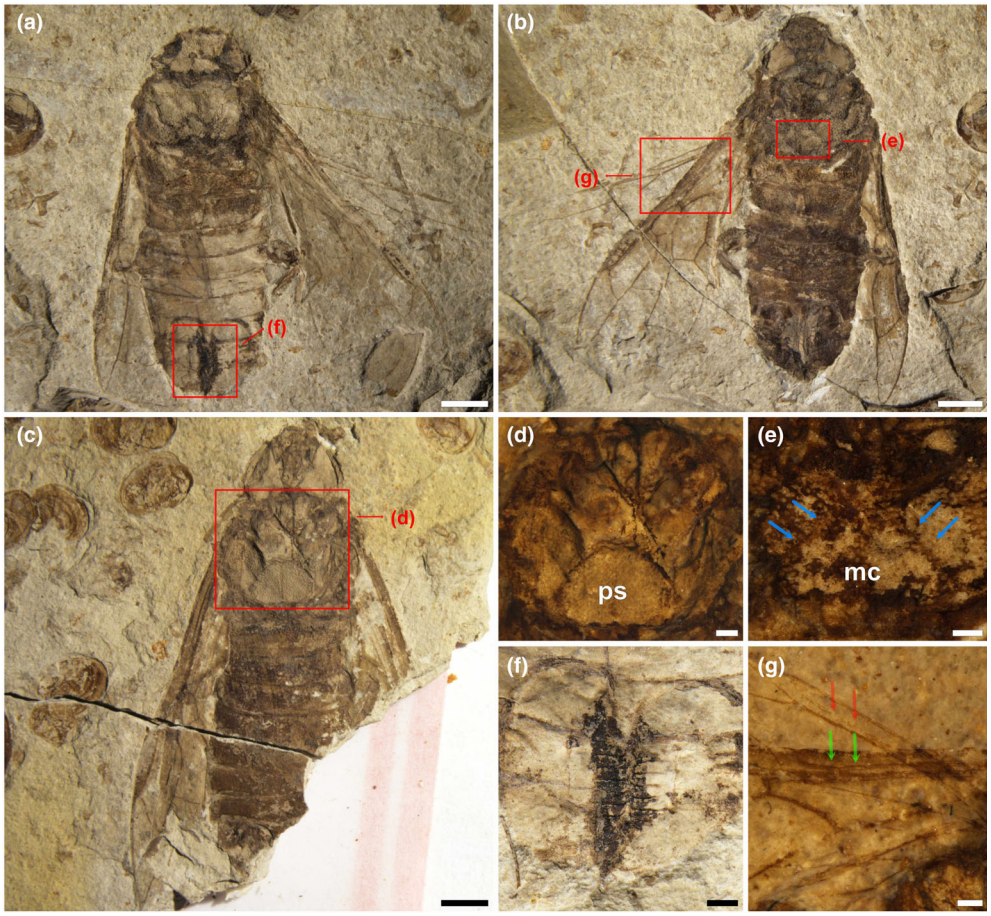

Fig. 8. †*Abrotoma robusta* and †*Xyelocerus* sp. (a) habitus, dorsal view of †*Abrotoma robusta*, CNU-HYM-NN2008014c. (b) habitus, ventral view of †*Abrotoma robusta*, CNU-HYM-NN2008014p. (c) habitus, ventral view of †*Xyelocerus* sp., CNU-HYM-NN2024031. (d) mesothorax under alcohol. (e) medioventral mesopleuron under alcohol. (f) ovipositor. (g) Sc in fore wing and hind wing under alcohol. Blue arrows mark the lateral grooves; green arrows mark vein Sc in fore wing; red arrows mark Sc in hind wing. Scale bars: 2 mm in (a–c); 0.5 mm in (d–g). mc, mesoscutellum; ps, pseudosternum.

mesothorax (Fig. S3e) with prescutum large and long, mesopseudosternal sulci developed (Fig. S3f).

Fore wing 6.5 mm in length and 2.7 mm in width, pterostigma nearly semicircular, completely sclerotized and nearly 2.6× as long as wide. Ovipositor 2.1 mm in length and 1.6 mm in width.

Paratype. CNU-HYM-LB2024005p/c (Fig. S4): Female. Body length 8.5 mm. Head (Fig. S4d) flat, 1.2 mm in length and 2.0 mm in width, antennal socket round. Clypeus developed and wide, its lower margin wavy. Antenna with at least nine segments. Mandible simple and forked, inner and outer teeth equal in length.

Thorax wider than head, cenchrus (Fig. S4c) developed and semicircular.

Fore wing 6.6 mm in length and 2.3 mm in width, pterostigma long, completely sclerotized and nearly 2.8× as long as wide.

Paratype. CNU-HYM-LB2024006p/c (Fig. S5): Female. Body length 9.7 mm. Head 1.6 mm long and 2.0 mm wide. Antenna at least 3 mm in length.

Thorax (Fig. S5c) with prescutum 0.6× as long as mesothorax, mesal mesoscutal sulcus developed and nearly reaching posterior end of notaulus. Mesoscutellum triangular and about a quarter of area of mesoprescutum, its lateral sulci meet in acute angle; mesoscutellar appendage absent.

Paratype. CNU-HYM-LB2024007 (Fig. S6): Female. Body length 9.8 mm. Head flat, 1.2 mm in length and 2.0 in width. Antenna (Fig. S6b) 10 segments and 2.7 mm in length, scape as wide as pedicel, first flagellomere nearly as long as following three flagellomeres combined.

Thorax (Fig. S6d) with mesoscutellum triangular, angle between the two lateral sulci less than 90°; mesoscutellar appendage absent.

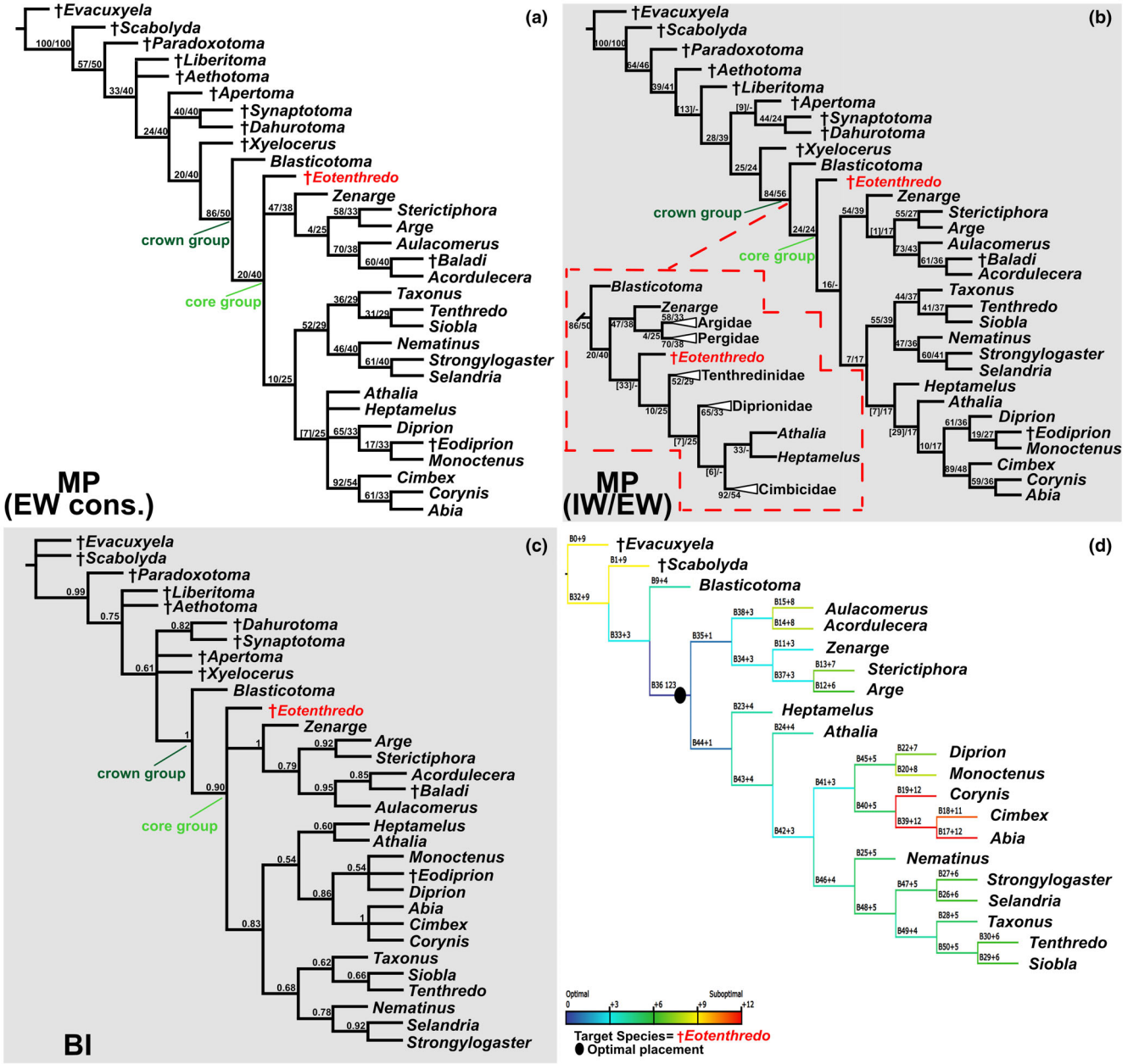

Fig. 9. Results of phylogenetic analyses. (a) Consensus tree derived from maximum parsimony (MP) analysis under equal weight (EW). (b) Implied weight (IW) most parsimonious tree (congruent with one of the two EW trees), and its differences from the other EW tree are shown in the dashed box with families that remain topologically unchanged collapsed. (c) Tree inferred in Bayesian inference (BI) analysis. (d) Result of running '*PlaceMyFossils*' for placing †*Eotenthredo* on a molecular reference tree from Wutke et al. (2024) based on MP criterion. Bootstrap values and relative Bremer support are shown in (a, b) next to relevant nodes. Posterior probabilities are shown in (c) near branches. The tag above the branch represents the score obtained by placing the target species on that branch in (d). '†'marks extinct taxa. '-'indicate no BR value on the branch. Abbreviations: cons. = consensus.

Fore wing 6.0 mm in length and 2.6 mm in width, 1-Rs weak (Fig. S6c).

Ovipositor (Fig. S6e) 2.1 mm in length and 1.7 mm in width, posterior part extending slightly beyond abdomen.

†Eotenthredo magna Zhuang, Wang, Vilhelmsen and Ren, sp. nov.

(Fig. 6, Fig. S7)

Material. Holotype, CNU-HYM-HP2024008, deposited in CNUB. Paratype, CNU-HYM-NN2024009 (CNUB).

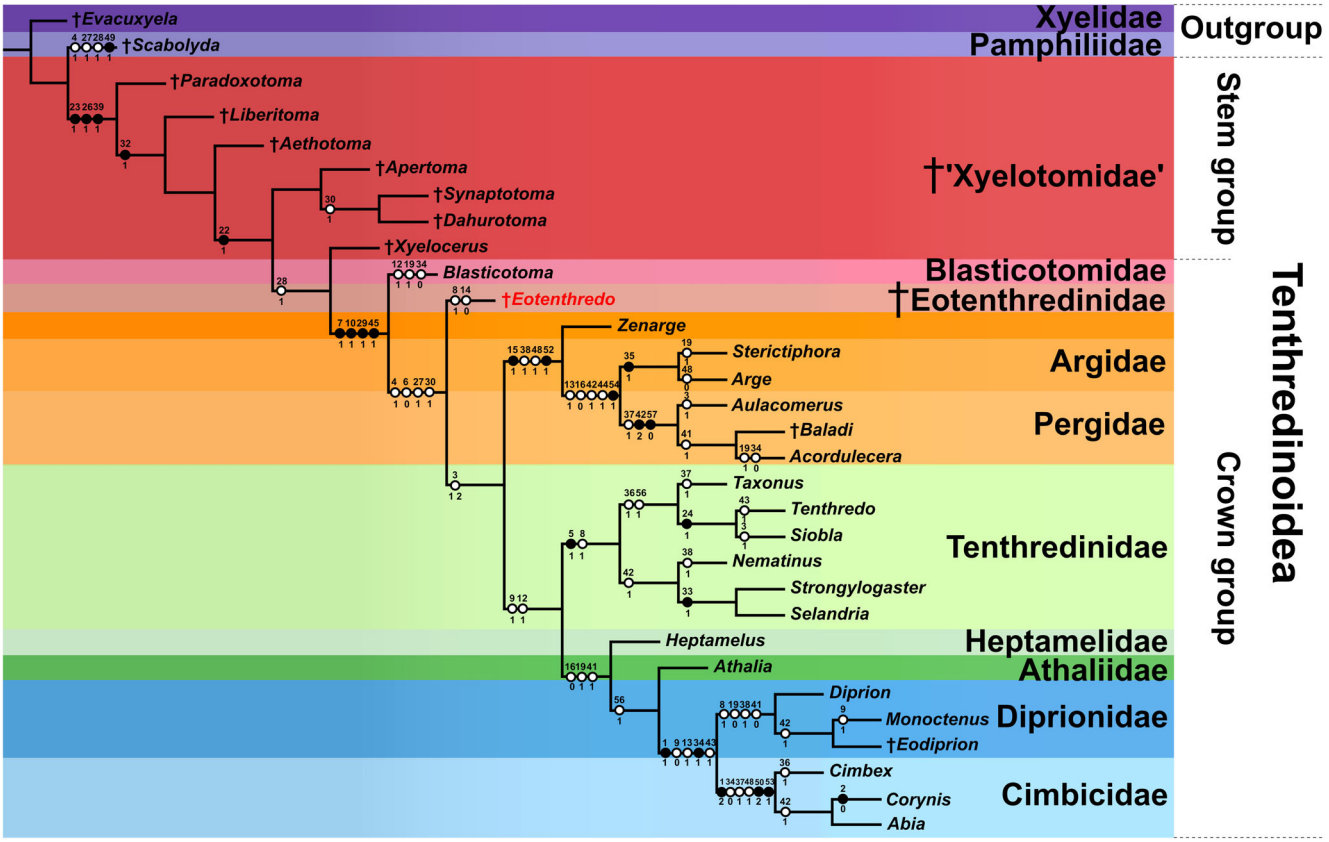

Fig. 10. Tree recovered from maximum parsimony (MP) analysis under EW with synapomorphic characters mapped. Tree length = 117. Unambiguous morphological character state changes are shown on the tree with a black circle indicating a homologous state and a white circle indicating a homoplasious state.

Diagnosis. Antenna with aspect ratio of each flagellomere less than 1.5, except first; fore wing with 1r-rs nearly half length of 2r-rs; Rs + M slightly shorter than 2-Rs; 2r-m entering cell 2mcu proximal to 2 m-cu.

Etymology. The specific name is derived from the Latin word 'magna', meaning large, referring to the larger body size compared to the other species in the genus.

Locality and horizon. Holotype: Yangshuling, Pingquan City, Hebei Province, China; Paratype: Liutiaogou, Chifeng City, Inner Mongolia. Yixian Formation, Lower Cretaceous.

Description. Holotype. CNU-HYM-LB2024008 (Fig. 6): Female. Body length 13.4 mm, head flat and subcircular, 2.1 and 2.8 mm in length and width, respectively. Antenna 11 segments and approx. 1.6× as long as head width. First flagellomere about 1.3 mm in length; combined lengths of remaining flagellomeres approx ca. 2.3× as long as first flagellomere (Fig. 6c).

Thorax considerably wider than head. Mesothorax with mesopseudosternum black (Fig. 6d). Legs partly preserved and coxae inverted trapeziform; hind leg at least 9.9 mm.

Fore wing (Fig. 6e) 9.8 mm in length and nearly 3.8 mm in width; pterostigma lanceolate and aspect ratio nearly 4; Sc developed and transverse, joining in R proximad to origin of Rs and distance between them nearly as long as 1r-rs. R bent at proximal end of Rs. M + Cu slightly curved; 1-M meeting 1-Cu at the angel of 78.6°; length proportions of vein Rs + M: 2-Rs: 1r-rs = 0.75: 0.68: 0.32; 3-Cu slightly longer than 1 m-cu. Angle between 2-Cu and 1 m-cu nearly 107.7°. Cell 3rm longer than 2rm and not markedly widened at apex; cell 1mcu ca. 1.2× as long as wide; cell 2a ca 4.1× as long as wide. Hind wing partly preserved with 1-Rs longer than 1-M; cell a blunt at apex.

Abdomen with ovipositor (Fig. 6b) approx. 3.2 mm long as preserved, very short and end slightly extending beyond abdomen.

Paratype. CNU-HYM-LB2024009 (Fig. S7): Female. Body length 13 mm. Head subcircular, 1.9 mm in length and 2.4 mm in width. Antenna partly preserved

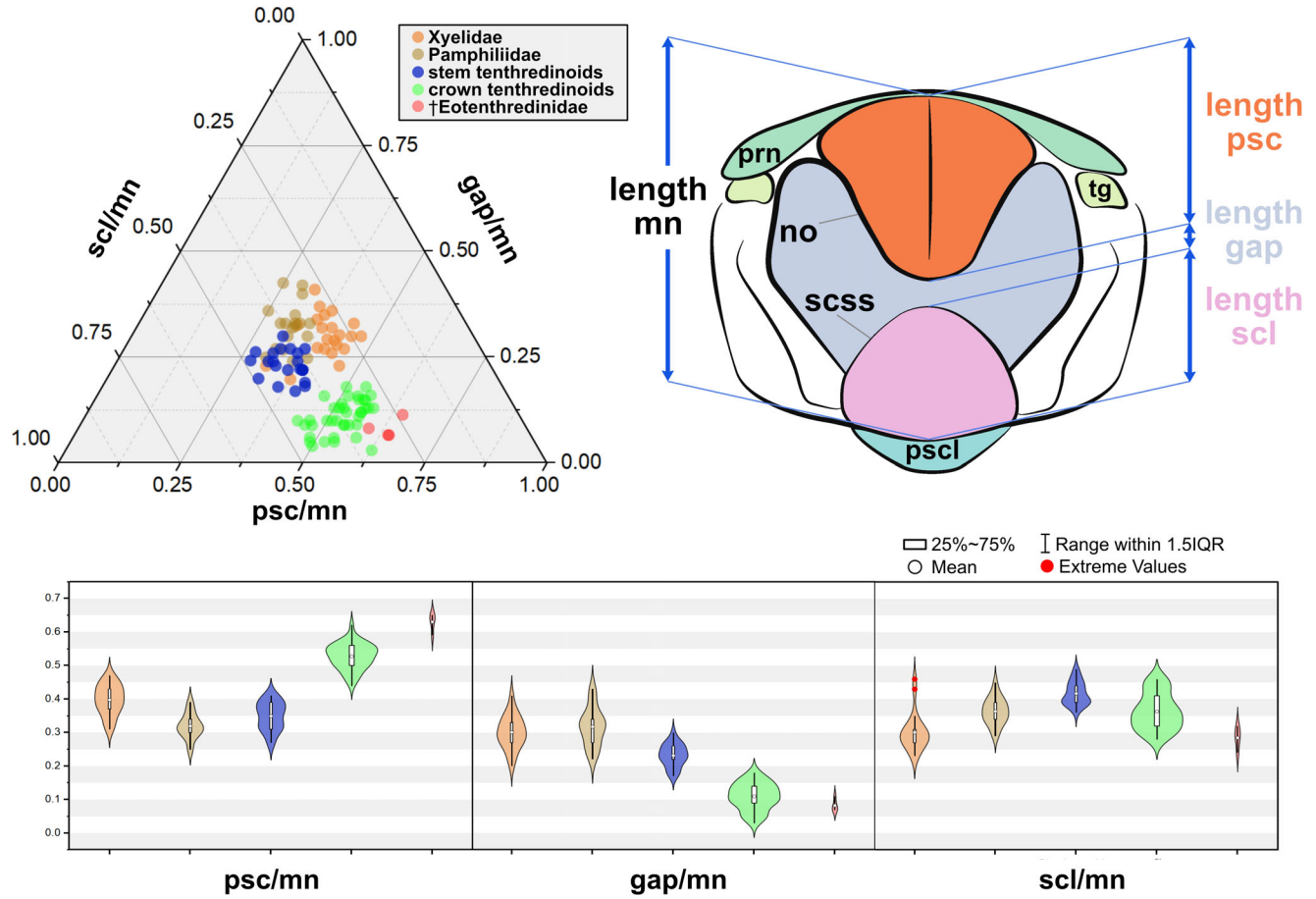

Fig. 11. Ternary diagram of measurements of the mesonotum (mn) elements (psc: prescutum; scl: scutellum; gap: the distance/gap between them) of sawflies. Violin plots show the distribution of the measured ratios for each group. The width of the box corresponds to the amount of data. mn, mesonotum; no, notaulus; prn, pronotum; psc, prescutum; pscl, postscutellum/mesoscutellar appendage; scl, scutellum; scss, scutum-scutellar suture; tg, tegula.

and the first flagellomere longer than half width of head (Fig. S7c).

Thorax considerably wider than head. Mesoprescutum longer than half length of mesothorax (Fig. S7d).

Fore wing 9 mm in length, Sc present and transverse, joining in R proximal to origin of Rs and distance between them nearly as long as 1r-rs. 1-M slightly bent and meeting 1-Cu in angle of 61.7°. Angle between 2-Cu and 1 m-cu 94.7°. Cell 1mcu approx. 1.3× as long as wide; cell 2a approx. 4.1× as long as wide.

Remarks. Besides the new genus, two other fossil taxa of uncertain familial placement have also been described from Early Cretaceous deposits: †*Atefia rasnitsyni* from the Crato Formation of Brazil (119.57–113.2 Ma; Krogmann et al., 2012) and †*Palaeathalia laiyangensis* from the Laiyang Formation of China (121.4–113.2 Ma; Zhang, 1985). Although the preserved characters of †*A. rasnitsyni* are limited, its bipectinate antennae suggest a distant relationship to the new genus. For †*P. laiyangensis*, it was considered to be a possible stem group athaliid because of the numerous plesiomorphic characters it displays, for example, long and slender antennae with more than 13 antennomeres, and a broader cell 1mcu with a short dorsal petiole (Niu et al., 2022). Additionally, the first flagellomere is similar in length to the second. This condition is in marked contrast to the much longer first flagellomere characteristic of our new genus. Overall, our new genus is clearly distinguishable from both †*Atefia* and †*Palaeathalia*.

In addition, we reviewed the published species of †'Xyelotomidae' and discovered that †*Leridatoma rudgwickensis* shares notable synapomorphies with †*Eotenthredo* in the fore wing, with the coastal area developed, Sc only developed as a crossvein, pterostigma nearly semicircular, 1-Rs absent and 2-Rs present, cell 1mcu nearly quadrangular, and 2A + 3A developed and not fused with 1A (Rasnitsyn et al., 1998). Based on these morphological affinities, we reassign this species to the genus †*Eotenthredo* as

†*Eotenthredo rudgwickensis* comb. nov. It can be distinguished from †*E. sinensis* and †*E. magna* by the curved M and R veins in the basal part of fore wing cell 3rm. Additionally, †*E. rudgwickensis* has fore wing with 2r-m entering cell 2mcu proximal to 2 m-cu (like †*E. magna*), whereas in †*E. sinensis* vein 2r-m posteriorly intersects 2 m-cu; Rs + M longer than 2-Rs (similar to †*E. sinensis*), vs. shorter than 2-Rs in †*E. magna*.

Phylogenetic analyses

The unconstrained MP analysis of the morphological data, under EW, yielded two most parsimonious trees (Fig. 9b, S21, CI = 0.58, RI = 0.83, length = 117 steps). The two most parsimonious trees differ mainly in the phylogenetic placements of †Eotenthredinidae, Heptamelidae and Athaliidae (see Fig. 9b), and their strict consensus tree is shown in Fig. 9a (CI = 0.56, RI = 0.82, length = 121 steps). Under IW with K = 12, the analysis produced a single most parsimonious tree (non-dashed part in Fig. 9b, Fig. S22, CI = 0.58, RI = 0.83, length = 117 steps), and its topology is the same as that of one of the most parsimonious trees recovered under EW. BS and BR values calculated under both weighting schemes are shown on the branches of the trees in Fig. 9a,b, respectively. In the unconstrained BI analysis, the inference analysis converged, and the posterior probabilities (PP) for each branch are shown in Fig. 9c. All of the unconstrained analyses recovered the new family with weak support or collapsed into a polytomy in these trees.

The constrained analysis, using the molecular backbone tree of Wutke et al. (2024) particularly with Heptamelidae and Athaliidae fixed, placed the new family as sister to the core tenthredinoids, which was the optimal placement inferred by the '*PlaceMyFossils*' script in TNT based on maximum parsimony criteria (Fig. 9d). In the EW analysis, we found that one of the two most parsimonious trees also recovered †Eotenthredinidae as the sister group to core tenthredinoids, and its topological structure is consistent with the results of the IW analysis. Therefore, we selected this tree (Fig. 9b, non-dashed part) as our preferred tree. It is presented separately as Fig. 10 for clarity in subsequent discussions. This tree was used for all downstream analyses, including the identification of synapomorphies, ancestral state reconstruction and LTT analyses.

Although multiple trees were generated using different methods (MP and BI), the relationships among key taxa remained stable across all analyses (Fig. 9a–c). Among them, Tenthredinoidea were recovered as monophyletic with strong support (BS = 100; BR = 100; PP = 0.99). The monophyly of †'Xyelotomidae' was not recovered; the genera formed a paraphyletic grade at the base of Tenthredinoidea with weak support for internal nodes. The crown tenthredinoids (Blasticotomidae, represented by *Blasticotoma* + †Eotenthredinidae, represented by †*Eotenthredo* + core tenthredinoids) were recovered as a monophyletic clade with good support (BS_{min} = 84; BR_{min} = 50; PP = 1).

Regarding the new genus †*Eotenthredo*, all analyses consistently placed it near the root of the core tenthredinoids. Support for this position was weak in the MP analyses (BSmin = 20; BRmin = 24) but relatively high in the BI analysis (PP = 0.90). The constrained analysis further recovered it as the sister group to core tenthredinoids (Fig. 9d). For the internal relationships of core tenthredinoids, two primary clades were recovered. One comprising *Zenarge* as sister to a clade containing Argidae and Pergidae, received moderate MP support (BSmin = 47; BRmin = 38) and strong BI support (PP = 1). The other formed by Tenthredinidae as sister to a clade encompassing Heptamelidae, Athaliidae and Diprionidae + Cimbicidae, albeit with weak support in the MP analyses (BS_{min} = 7; BR_{min} = 17), but with moderate support in the BI analysis (PP = 0.83).

Synapomorphies supporting the key nodes identified in our analysis are presented in Fig. 10. The monophyly of Tenthredinoidea is supported by the fore wing having the widest part of the coastal area located at the origin of 1-Rs, M + Cu slightly curved or straight, 2r-rs entering cell 3rm (char. 23: 1, 26: 1, 39: 1). The monophyly of crown tenthredinoids is supported by the anterior margin of the mesoprescutum noticeably curved in the middle, the length of mesoprescutum being longer than half length of mesothorax, the fore wing with 1-Cu less than 1.5× the length of 1-M, and the wing with Sc absent (char. 7: 1, 10: 1, 29: 1, 45: 1). The node, including core tenthredinoids and †*Eotenthredo*, lacked synapomorphies despite the presence of four homoplasies. Similarly, the node 'core tenthredinoids' also lacks synapomorphies. Of the two primary clades in core tenthredinoids, only (*Zenarge* + Argidae + Pergidae) is supported by the anepimeron anteriorly expanded and dorsally convex, and the second valvifer and 3rd valvula totally fused (char. 15: 1, 52: 1).

Statistical analysis of the mesothorax

The ternary diagram of the mesothoracic proportions (Fig. 11) shows that Xyelidae, Pamphiliidae and stem tenthredinoids cluster centrally, indicating a broadly similar mesothoracic configuration. In contrast, crown tenthredinoids and †Eotenthredinidae form a separate cluster near the lower edge of the diagram, reflecting their smaller gap/mn ratios.

Violin plots of psc/mn reveal clear separation among groups: Xyelidae, Pamphiliidae and stem tenthredinoids show ratios concentrated between 0.3 and 0.45;

crown tenthredinoids cluster between 0.5 and 0.55; and †Eotenthredinidae displays an even higher value 0.63. Violin plots of gap/mn further differentiate the groups: Xyelidae, and Pamphiliidae clusters between 0.25 and 0.35, stem tenthredinoids between 0.2 and 0.3, crown tenthredinoids between 0.1 and 0.15, and †Eotenthredinidae near 0.07. Finally, violin plots for scl/mn show that Xyelidae and †Eotenthredinidae have similar ratios (≈0.25 and 0.3), whereas Pamphiliidae, stem tenthredinoids and crown tenthredinoids span slightly higher values (0.3 and 0.45).

Ancestral state reconstruction and heatmap

A first-to-second flagellomere length ratio >3 is commonly observed in many Mesozoic sawfly species (a plesiomorphic condition and possibly a hymenopteran ground plan trait, Rasnitsyn, 1996; Wang et al., 2013). Both outgroups (Xyelidae and Pamphiliidae) and the ancient tenthredinoids (i.e. †'Xyelotomidae' and Blasticotomidae) have a ratio >3. In the sister group of core tenteredinoids, viz. †*Eotenthredo*, this plesiomorphic ratio is retained.

Our ancestral state reconstruction (Fig. 12) indicates that the evolution of the relative length of the first flagellomere within core tenthredinoids proceeded along two main trajectories towards shortening. In the (*Zenarge* + Argidae + Pergidae) clade, the ancestral state was likely an elongate first flagellomere, combined with the loss of the second flagellomere. A reduction of the first flagellomere length subsequently occurred in Pergidae. In the second lineage (Tenthredinidae + Heptamelidae + Athaliidae + Diprionidae + Cimbicidae), the ancestral condition appears to have involved initial shortening (ratio ca. 1.5–3), followed by further reduction in Tenthredinidae to <1.5.

The heatmap analysis highlights lineage-specific variations in first flagellomere proportions. Despite lacking a second flagellomere, Argidae possess an even more elongate first flagellomere than stem tenthredinoids, approaching the level of elongation observed in the composite first flagellomere of Xyelidae. The heatmap also indicates a general trend in which the shortening of the first flagellomere correlates with the lengthening of the second flagellomere, a trend particularly evident in Tenthredinidae. Diprionidae, however, deviate from this overall trend.

Lineages of plants and composition of fossil tenthredinoids through time

The LTT plots illustrate the changes in diversity of angiosperms, gymnosperms, and pteridophytes over time (Fig. 13). The diversity of angiosperms began to increase in the Early Cretaceous, rose sharply between the Late Cretaceous and the mid-Paleogene, then reached a secondary peak at the beginning of the Neogene, and decline through the Neogene to the present. By contrast, the diversity of pteridophytes and gymnosperms was comparatively low and stable since the Triassic, only fluctuating slightly, and with a slight decline in pteridophytes (Fig. 13).

For tenthredinoids, the fossil record of the stem group (†'Xyelotomidae') is concentrated in the Jurassic-Cretaceous, with no records thereafter. In contrast, the evolutionary history of the crown group shows distinct phases: they first appeared in the Cretaceous, but with low diversity—only †Eotenthredinidae, †*Palaeathalia laiyangensis* (perhaps belonging to Athaliidae) and †*Atefia rasnitsynias* have been described from this period. During the Paleogene, the number of fossil species increased sharply. Eight of the 10 crown-group tenthredinoid families are documented in the fossil record, indicating a marked rise in familial diversity approaching modern levels. By the Neogene, the number of fossil species declined somewhat, with fossils from four of the 10 families discovered.

Discussion

The evolutionary history of Tenthredinoidea has traditionally been reconstructed primarily through the lens of extant taxa, leaving the definition and evolutionary dynamics of the Early Mesozoic lineages poorly understood. This gap in our understanding of tenthredinoid evolution is largely attributable to the scarcity of relevant fossils. Our study bridges this knowledge gap by integrating, for the first time, an extensive dataset of the Mesozoic fossils into phylogenetic reconstructions. This includes the newly discovered and described oldest known crown-group tenthredinoids. This deep-time perspective enables a reconstruction of the group's morphological diversification from its origins and a reassessment of its internal relationships and potential evolutionary interaction with plants.

Systematics and relationships among Tenthredinoidea

†'Xyelotomidae' and Blasticotomidae. †'Xyelotomidae' represent the stem group of Tenthredinoidea. They are first recorded from the Lower Jurassic and are characterized by a first flagellomere typically at least twice as long as the thread and significantly thicker, a fore wing with Sc stalk usually present and a 1-Rs vein developed in most cases.

Due to the scarcity of well-preserved fossils and available morphological data, systematic studies of †'Xyelotomidae' have been rare. Ronquist et al. (2012) and Zhang et al. (2016) included representatives of

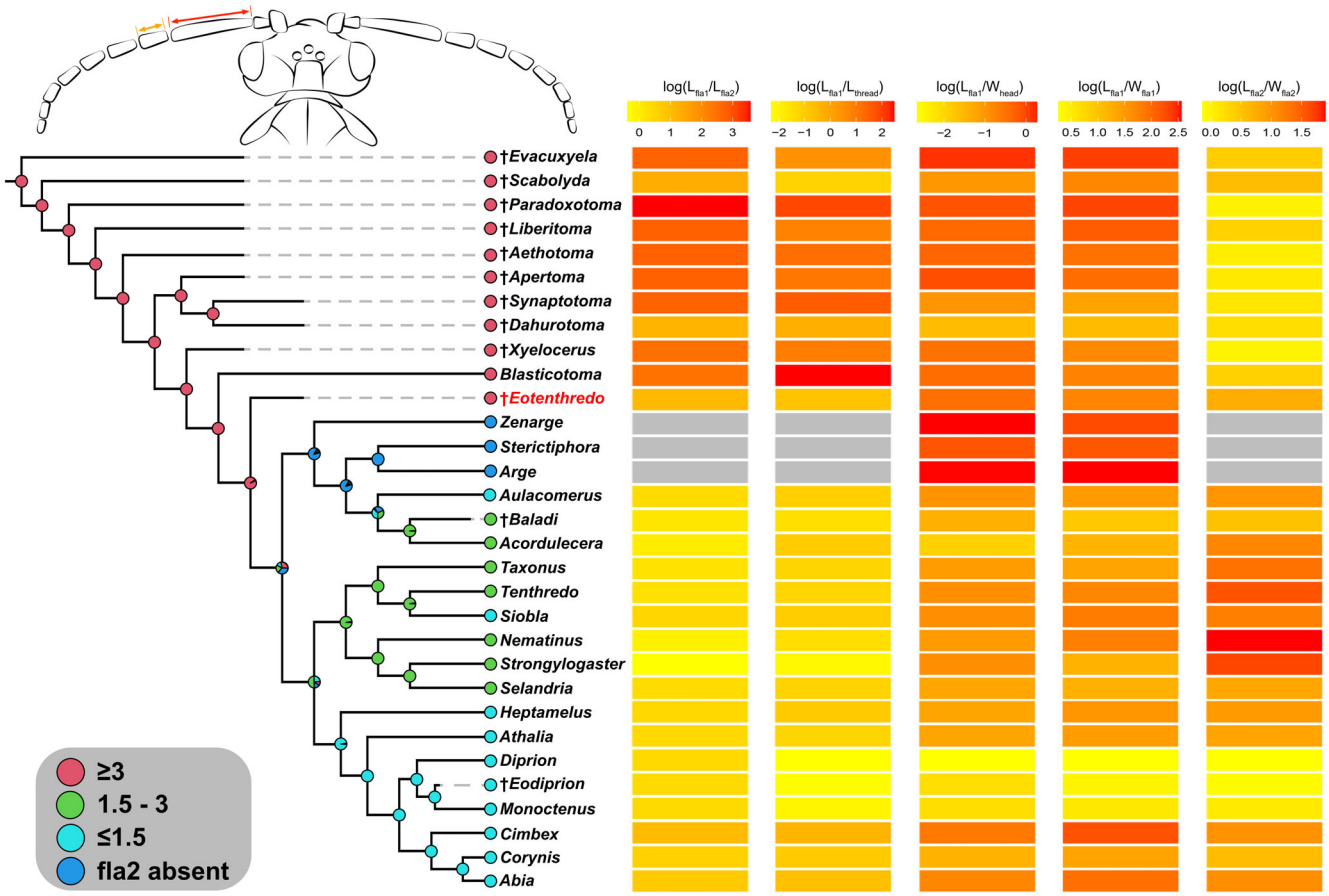

Fig. 12. Ancestral state estimation of the ratio of the first flagellomere to the second based on the MAP tree. Circles depict character states for tips or nodes. Heatmaps show log ratios between the length of fla_1 and fla_2; the length of fla_1 and thread (viz. flagellomeres except the first one); the length of fla_1 and the width of head; the length of fla_1 and the width of fla_1; length of fla_2 and the width of fla_2 in turn. Each heatmap is on a unique numerical scale to maximize visibility. Grey cells in the heatmaps depict missing data. Ancient taxa tend to have a long (large aspect ratio) first flagellomere and a short (small aspect ratio) second flagellomere.

xyelotomids in their early Hymenoptera radiation analyses; their results, consistent with ours, recovered †'Xyelotomidae' as paraphyletic, albeit with poor resolution (Ronquist et al., 2012, fig. 7). Recently, Rasnitsyn and Müller (2023) proposed synonymizing †'Xyelotomidae' with Blasticotomidae citing similarities in larval and adult morphologies; however, this taxonomic hypothesis remains untested through phylogenetic analysis.

Our results (Fig. 10) corroborate earlier views (Rasnitsyn, 1969; Nel et al., 2004); xyelotomids emerge as paraphyletic rather than monophyletic, representing an assemblage of stem groups to crown Tenthredinoidea; however, the nodes are weakly supported.

Blasticotomidae, here represented only by *Blasticotoma*, are characterized by a very long first flagellomere with at most one short additional flagellomere present, and a fore wing without Sc. The earliest fossils of the family are dated back to the Eocene (Table S1). Blasticotomidae are clearly placed as a member of crown tenthredinoids with good support. Characters supporting this placement include the following: the noticeably curved anterior margin of the mesoprescutum, a developed mesoprescutum (longer than half the length of the mesothorax), the shortened vein 1-Cu (1-Cu: 1-M < 1.5), and the absence of vein Sc in the hind wing. Therefore, we consider it useful to retain †'Xyelotomidae' as an informal group for Mesozoic stem group tenthredinoids rather than synonymizing it with Blasticotomidae.

†Eotenthredinidae fam. nov. The new family †Eotenthredinidae is recovered near the base of the core tenthredinoids in the unconstrained analysis, albeit with moderate support (Fig. 9a–c). In the constrained analysis, it is inferred to be the sister group to core Tenthredinoidea (Fig. 9d). This placement is corroborated by a mosaic of ancestral and derived traits that illuminate early crown-group morphology.

†Eotenthredinidae retains notable plesiomorphies, such as an elongate first flagellomere (at least three

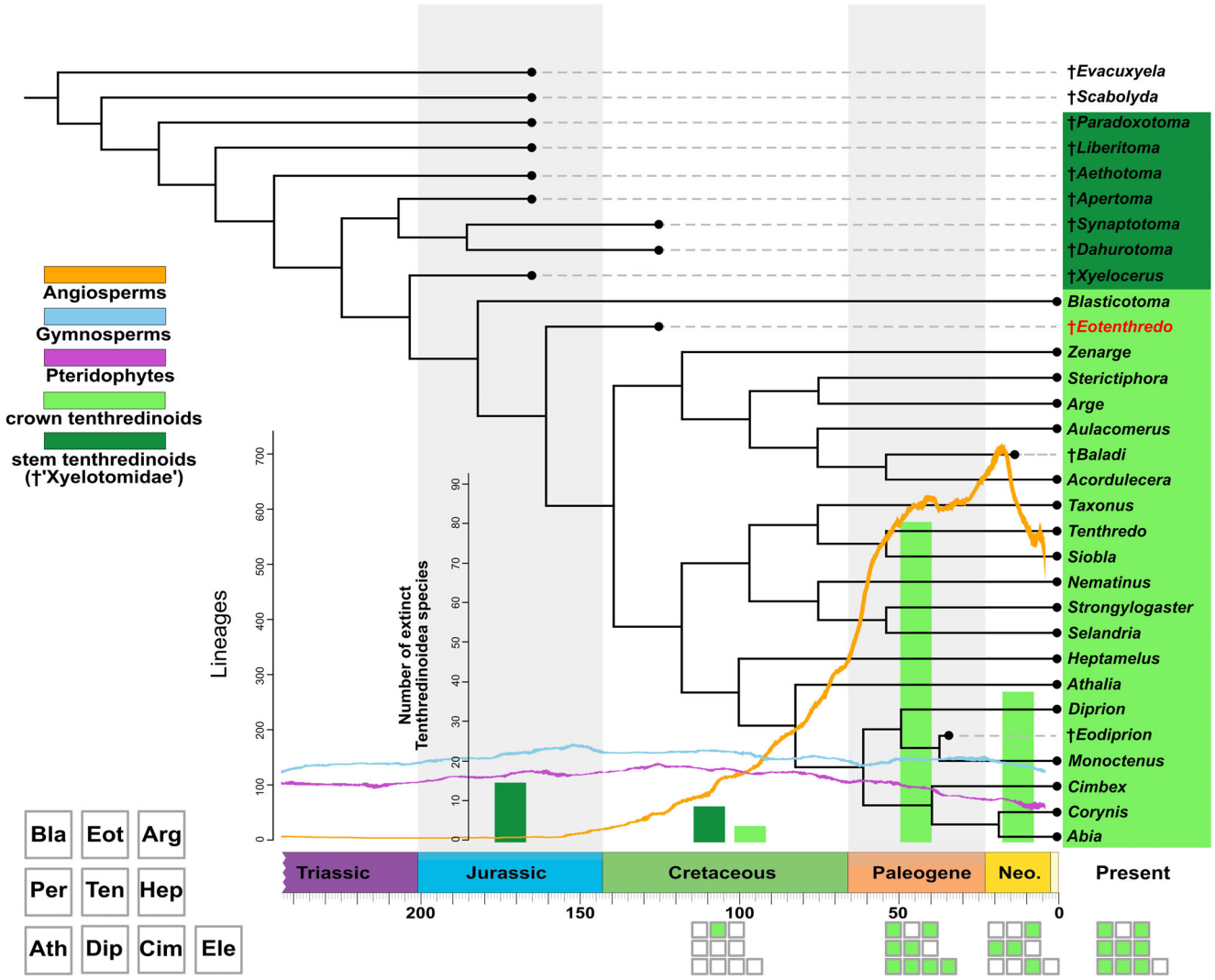

Fig. 13. Phylogeny of Tenthredinoidea. The orange, blue and purple curves represent the lineages through time of angiosperms, gymnosperms and pteridophytes separately. The leftmost vertical axis shows the numbers of lineages of plants. The light green and dark green represent crown and stem tenthredinoids separately. The vertical axis of the second column on the left shows the number of fossils in the corresponding geological periods. The ten-grid chart corresponds precisely to all families within the crown tenthredinoids, and they are coloured once they appear during the corresponding period. It should be emphasized that, in the cladogram, only the time of the terminal nodes corresponds to the time scale at the bottom, whereas the ages of the internal nodes do not. Family abbreviations, in sequential order from left to right, are provided in the bottom-left corner: Arg, Argidae; Ath, Athaliidae; Bla, Blasticotomidae; Cim, Cimbicidae; Dip, Diprionidae; Ele, †Electrotomidae; Eot, †Eotenthredinidae; Hep, Heptamelidae; Per, Pergidae; Ten, Tenthredinidae.

times the length of the second), a narrow triangular mesoscutellum (left and right scutoscutellar sulcus meeting in an acute angle, the width of mesoscutellum less than half of mesoprescutum), and an anteriorly abbreviated mesopseudosternal sulcus (meeting before the anterior margin of the mesopleuron). The retention of these traits, which are characteristic of stem tenthredinoids and also of xyeloids, is congruent with its inferred basal position within the crown group.

Conversely, it also displays derived characters. The evenly thickened flagellomeres and the first flagellomere, which is shorter than the combined length of the rest, may represent two potential synapomorphies uniting †Eotenthredinidae with core Tenthredinoidea, despite the possible homoplastic origin of this trait across Hymenoptera (Rasnitsyn, 1988; Ronquist et al., 1999; Vilhelmsen, 2001). Additionally, the new family possesses a quadrilateral cell 1mcu and lacks 1-Rs in the fore wing, both of which are typical characters of extant core tenthredinoids.

This morphological mosaic is further corroborated by our quantitative morphometric analyses of the mesothorax (Fig. 11). They show that †Eotenthredinidae clusters with crown tenthredinoids, occupying a

distinct morphospace separate from the stem tenthredinoids and other sawflies, primarily due to its significantly increased psc/mn and reduced gap/mn ratio. Meanwhile, its scl/mn ratio remains more similar to that of Xyelidae in violin plots.

In summary, the mosaic combination of morphological characters in †Eotenthredinidae, as well as its phylogenetic position outside any extant families, provides robust justification for the establishment of the new family. Moreover, this mosaic pattern, which mixes ancestral and derived states, indicates that †Eotenthredinidae may represent an independent early diverging branch within the crown group, not a member of the later core radiation.

Extant core tenthredinoids. Morphology-based phylogenetic framework for extant core tenthredinoids has long been hampered by extensive morphological diversity, which obscures groundplan character states, particularly within the species-richest family Tenthredinidae (Vilhelmsen, 2001; Schulmeister, 2003). Recent molecular studies (Malm and Nyman, 2015; Niu et al., 2022; Wutke et al., 2024) have indicated two major clades: Argidae + Pergidae, predominantly distributed in the Southern Hemisphere, and Heptamelidae + (Athaliidae + ((Cimbicidae + Diprionidae) + Tenthredinidae)).

The results of our unconstrained phylogenetic analysis (Figs 9a–c and 10) are largely congruent with the topology recovered by Wutke et al. (2024). However, some nodes, especially within Tenthredinidae, received low support, a common limitation in morphology-only analyses. Similarly, the positions of Heptamelidae and Athaliidae remain ambiguously supported. Nonetheless, our analysis moderately supports *Zenarge* as the sister to the Argidae + Pergidae clade, consistent with the results of Malagón-Aldana et al. (2021, 2022).

Although the incorporation of numerous stem tenthredinoids in our dataset clarifies several ancestral character states, internal relationships among extant core tenthredinoid taxa remain weakly supported. The limitations likely stem from restricted taxon sampling and inherent biases in character selections due to incomplete preservation in fossil specimens (Pattinson et al., 2015). Future fossil discoveries, especially well-preserved fossils and integrated molecular datasets, will be crucial to resolving character-poor and problematic taxa and refining the evolutionary framework of Tenthredinoidea.

It is also worth noting that support values for several nodes differed between the MP and BI analyses. Support values were generally lower in the MP analyses than in the BI analysis, reflecting methodological differences. Parsimony methods tend to yield conservative support values in datasets with missing data and homoplasy, as such ambiguity reduces the strength of the test of character congruence (Nixon, 1996). In contrast, Bayesian inference under the Mk model may better accommodate rate heterogeneity among characters and often produces more robust trees (Spencer and Wilberg, 2013).

Early evolution and diversity of Tenthredinoidea

The early evolutionary framework of Tenthredinoidea was first outlined by Rasnitsyn (1969, 1980). He proposed that the superfamily appeared no later than the Middle Jurassic, being represented by †'Xyelotomidae'. †'Xyelotomidae' subsequently diversified into three lineages: (i) Blasticotomidae, the earliest-diverging branch retaining numerous pleisomorphies; (ii) †Electrotomidae + Argidae + Pergidae, with †Electrotomidae as the earliest representative; and (iii) Tenthredinidae + Cimbicidae + Diprionidae, the lineage comprising the greatest variety, wherein Tenthredinidae was the most basal family and gave rise to the latter two. As inferred from fossil evidence, the first two lineages diverged early, whereas the third group arose during the Mid- to Late Cretaceous. These early evolutionary patterns have since been supported by divergence time estimates from recent phylogenomic analyses (Wutke et al., 2024).

Our study (Fig. 13) is generally consistent with Rasnitsyn's hypothesis regarding the early evolution of Tenthredinoidea. However, phylogenetic results demonstrate that lineages ii and iii are sister groups. By definition, they diverged at the same time, which is now firmly established in the evolutionary framework of Tenthredinoidea (Ronquist et al., 2012; Wutke et al., 2024).

Furthermore, †Eotenthredinidae, as one of the currently oldest lineage of crown tenthredinoids from the Mesozoic era, provides direct evidence for the early divergence of the superfamily. Its mosaic of morphological characteristics—combining plesiomorphic traits with definitive crown-group synapomorphies—demonstrates that the differentiation of the crown group, and even the core tenthredinoids, occurred no later than the Early Cretaceous (~125 Ma). During this period, mesothoracic structures had already undergone significant modification within the crown group, such as the noticeably curved anterior margin of the mesoprescutum (viz. the deeply curved posterodorsal margin of the pronotum) and the elongated mesoprescutum (longer than half the length of the mesothorax). Regarding the shortening of the first flagellomere, it appears to have been a complex evolutionary process with multiple independent origins. This is reflected in the considerable variation in first flagellomere length observed across extant core tenthredinoids (Fig. 12). We acknowledge that the true extent of morphological variation in this trait within the clade is greater than captured by our currently limited taxon sample,

especially in extant families. Future studies with denser sampling are needed to refine the precise evolutionary trajectory of flagellar morphology.

Evolutionary association between Tenthredinoidea and plants

The evolutionary history of Tenthredinoidea is closely linked to plants, particularly angiosperms (Nyman et al., 2006). This association is reflected in specialized ovipositors and the diversified herbivorous habits of the larvae (Nyman et al., 2006; Leppänen et al., 2012). While the close link between tenthredinoid diversification and angiosperms is already well-established (Isaka and Sato, 2014; Nyman et al., 2019), the fossil record provides direct evidence for testing and calibrating this macroevolutionary narrative. Here, we try to unravel the deep-time dynamics of this key association from the fossil perspective.

A key morphological innovation in the Jurassic: the highly sculptured ovipositor. Ovipositor morphology and oviposition behaviour have played crucial roles in hymenopteran evolution (Gauld and Bolton, 1988). Sawflies and wasps have diverse ovipositor forms enabling egg deposition in a range of substrates or hosts (Quicke, 1997; Vilhelmsen, 2000; Weltz and Vilhelmsen, 2014). In †*Xyelocerus diaphanus* and †*Abrotoma robusta*, species of †'Xyelotomidae' from the late Middle Jurassic, distinct oblique ridges can be seen on the surface of ovipositors (Figs 7 and 8). This structure contrasts with the ridgeless or weakly ridged ovipositors of Xyelidae, suggesting a critical transition in oviposition strategy from laying the eggs externally to pushing them into the host plant to more effectively cut inside the plant tissues before placing the egg (Burdick, 1961; Weltz and Vilhelmsen, 2014; Blank et al., 2017). Evidence from coevolving plant fossils showing insect oviposition damage (damage type 181, Xiao et al., 2024) supports this behavioural transition.

The oblique ridges and generally complex sculpture on the ovipositor increase the penetrating capacity of the ovipositor, allowing eggs to be inserted deeply inside plant tissues, which protects them and ensures immediate proximity to the food source, thereby enhancing larval survival (Hinton, 1981; Feng et al., 2022; Romero-Lebrón et al., 2022). This innovation reflects the establishment of an intimate ecological relationship between tenthredinoids and their host plants from the start.

The diversification of crown tenthredinoids and radiation of angiosperms. The fossil record provides direct evidence for a macroevolutionary trajectory of Tenthredinoidea that is closely coupled with the rise of angiosperms. While the fossil record is inevitably influenced by bias, the overall pattern illustrated by the LTT plots of plants and family level fossil composition of Tenthredinoidea shows a clear shift (Fig. 13).

The stem tenthredinoids, †'Xyelotomidae', are the sole representatives of the superfamily during the Jurassic but have no fossil record after the Lower Cretaceous (Rasnitsyn, 1988). During this period, plant communities were dominated by gymnosperms, with ferns being a significant but subordinate component (Labandeira, 2014; Xiao et al., 2025). Nyman et al. (2019) optimized gymnosperm feeding as ancestral for Hymenoptera, with Tenthredinoidea switching to angiosperm feeding in their ground plan. However, they were only concerned with extant taxa and the inference may only apply to the most recent common ancestor of the extant tenthredinoids, viz. crown group, and does not necessarily extend to the stem lineages. Given the temporal and ecological context, the stem lineages of Tenthredinoidea possibly fed primarily on gymnosperms, and an alternative association with ferns cannot be ruled out. The decline of the 'xyelotomid' lineages in the Upper Cretaceous may have been influenced by significant plant community changes marked by the rise of angiosperms. It has to be acknowledged that the fossil record does not currently allow for a precise determination of when the shift to angiosperm feeding took place within the Tenthredinoidea, only that it probably happened prior to the radiation of the crown group (see Nyman et al., 2019).

In contrast, crown tenthredinoids first appeared in the Cretaceous, ca. 125 Ma, but with very low diversity, represented by †Eotenthredinidae during this period. Their first appearance is temporally close to that of the earliest angiosperms in the fossil record (Sun et al., 1998, 2002; Friis et al., 2003). More importantly, †Eotenthredinidae are preserved in the same strata (Yixian Formation) as some of these earliest flowering plants, such as †*Archaefructus* (Sun et al., 1998, 2002). Although it cannot be confirmed whether a direct link existed between them at this stage, this temporal and spatial association suggests that these taxa shared the same paleoenvironment, potentially providing a foundation for later long-term co-evolutionary relationships.

In the Paleogene, a pivotal diversification pulse for the crown tenthredinoids clearly happened (Fig. 13). The crown-group tenthredinoid fossil record from this interval shows a sharp increase in the number of fossil species and documents the majority of the 10 crown-group families (eight out of the 10 families), approaching modern familial diversity. This rapid rise in lineage richness occurred just after angiosperm diversity had increased sharply, suggesting the close association was well-established by this time.

The potential biases in fossil record. It should be noted that the observed fossil diversity pattern may be

influenced by several biases inherent to the fossil record, especially limited tenthredinoid fossils. The 'Lagerstätten effect' can inflate diversity in specific intervals by preserving taxa that overcompensate with taxa from one geographic area or timeframe (Woolley et al., 2024). There is no doubt that this may hinder diversity studies that require uniform sampling across space and time (Walker et al., 2019). Additionally, collection and expertise biases may overrepresent or overlook certain families due to sustained research interest or differential sampling intensity (Battista and Schultz, 2024). For example, the tenthredinoid fossil record is heavily skewed towards the Northern Hemisphere, with few studies from the Southern Hemisphere where extant families such as Argidae and Pergidae are diverse today (Wutke et al., 2024). While these biases preclude strong quantitative inferences, our integrated analysis, considering the number of fossil species, familial diversity and co-occurrence pattern in geological strata, reveals a likely genuine macroevolutionary signal that tracks association between angiosperms and true sawflies. Future discoveries and more comprehensive sampling will help to refine this framework.

In summary, the fossil record delineates a clear macroevolutionary process: The decline of the stem tenthredinoids and the rise of crown tenthredinoids could be related to the rise of angiosperms, and the major radiation of Tenthredinoidea was possibly synchronized with the peak diversification of flowering plants in the Paleogene. This potential correlation indicates that the KTR, and specifically the ecological expansion of angiosperms, provided the fundamental macroevolutionary opportunity that catalysed the radiation of the core tenthredinoid lineages.

This deep-time co-evolutionary pattern was not unique to Tenthredinoidea; comparable interactions occurred across other insect groups, such as beetles, bugs and brachycera flies, that acted as early angiosperm pollinators or consumers during the Cretaceous (Ren, 1998; Bao et al., 2019; Peris et al., 2020; Boderau et al., 2025). Together, these interactions contributed to the KTR and the restructuring of modern terrestrial ecosystems.

Conclusion

We describe the oldest crown tenthredinoids: †Eotenthredinidae fam. nov., containing †*Eotenthredo sinensis* gen et sp. nov.; †*E. magna* sp. nov., from the Early Cretaceous Yixian Formation of China. †Eotenthredinidae represents a key transitional taxon, combining apomorphic and plesiomorphic traits, contributing to illuminate an important stage in the morphological evolution of Tenthredinoidea.

Our phylogenetic analyses, incorporating a comprehensive sampling of Mesozoic fossil genera, support the monophyly of Tenthredinoidea and demonstrate that †'Xyelotomidae' is paraphyletic and should not be synonymized with Blasticotomidae. †Eotenthredinidae is recovered as the sister group to the core tenthredinoids. Although the support for this specific node is moderate, this likely reflects well-known limitations of morphology-based phylogenetic reconstructions, particularly in the context of rapid radiation events. The recognition of †Eotenthredinidae as a well-defined morphologically distinct lineage provides a crucial anchor point for future total-evidence analyses.

Overall, this study provides novel paleontological evidence and an evolutionary framework that deepens our understanding of the early diversification of Tenthredinoidea and its synergistic relationship with plants, especially the rise of angiosperms during the Cretaceous Terrestrial Revolution.

Acknowledgements

We are grateful to the editor, John M. Heraty, and the reviewers for their valuable suggestions and comments, which helped improve this manuscript. Jialiang Zhuang is grateful to Zhen Wang, Ziqiang Xu, Jiawei Chao and Rui Dai (all from Capital Normal University) for their help. In this work, Mei Wang was supported by the Fundamental Research Funds for the Central Non-profit Research Institute of Chinese Academy of Forestry (Grant No. CAFYBB2024Q G005). Dong Ren was supported by the National Key R & D Program of China (No. 2025YFF0811700), the National Natural Science Foundation of China (42288201, 42472001).

Conflict of interest

The authors declare that there is no conflict of interest.

Data availability statement

The data that supports the findings of this study are available in the supplementary material of this article.

References

Bao, T., Wang, B., Li, J. and Dilcher, D., 2019. Pollination of Cretaceous flowers. Proc. Natl Acad. Sci. USA 116, 24707–24711.

Battista, F. and Schultz, C.L., 2024. Sampling and collector biases as taphonomic filters: an overview. An. Acad. Bras. Cienc. 96, e20231242.

Benton, M.J., Wilf, P. and Sauquet, H., 2022. The angiosperm terrestrial revolution and the origins of modern biodiversity. New Phytol. 233, 2017–2035.
Blank, S.M., Kramp, K., Smith, D.R., Sundikov, Y.N., Wei, M. and Shinohara, A., 2017. Big and beautiful: the *Megaxyela* species (Hymenoptera, Xyelidae) of East Asia and North America. Eur. J. Taxon. 348, 1–46.
Boderau, M., Nel, A. and Jouault, C., 2025. Diversification and extinction of Hemiptera in deep time. Commun. Biol. 8, 352.
Burdick, D.J., 1961. A taxonomic and biological study of the genus *Xyela* Dalman in North America. Uni. Cal. Publ. Entomol. 17, 285–355.
Catalano, S.A., Escapa, I., Pugh, K.D., Hammond, A.S., Goloboff, P. and Almécija, S., 2025. PlaceMyFossils: an integrative approach to analyze and visualize the phylogenetic placement of fossils using backbone trees. Syst. Biol. 74, 672–684.
Ding, W.N., Silvestro, D., Onstein, R.E., Wu, M.X., Zhou, Z.K. and Xing, Y.W., 2025. The stepwise rise of angiosperm-dominated terrestrial ecosystems. Biol. Rev. 100, 2131–2149.
Feng, Z., Wan, S., Sui, Q., Labandeira, C., Guo, Y. and Chen, J.B., 2022. A Triassic tritrophic triad documents an early food-web cascade. Curr. Biol. 32, 5165–5171.
Feng, Q., Zhou, C.X., Jiang, R.X., Shih, C.K., Ren, D. and Wang, Y.J., 2025. The earliest fossil sheds light on the evolution of vermileonid flies. Insect Syst. Divers. 9, ixaf036.
Friedman, W.E., 2009. The meaning of Darwin's "abominable mystery". Am. J. Bot. 96, 5–21.
Friis, E.M., Doyle, J.A., Endress, P.K. and Leng, Q., 2003. *Archaefructus* – angiosperm precursor or specialized early angiosperm? Trends Plant Sci. 8, 369–373.
Gauld, I. and Bolton, B., 1988. The Hymenoptera. Oxford University Press, Oxford, UK.
Goloboff, P.A. and Catalano, S.A., 2016. TNT version 1.5, including a full implementation of phylogenetic morphometrics. Cladistics 32, 221–238.
Goloboff, P.A., Torres, A. and Arias, J.S., 2018. Weighted parsimony outperforms other methods of phylogenetic inference under models appropriate for morphology. Cladistics 34, 407–437.
Harmon, L.J., Weir, J.T., Brock, C.D., Glor, R.E. and Challenger, W., 2008. GEIGER: investigating evolutionary radiations. Bioinformatics 24, 129–131.
Hinton, H.E., 1981. Biology of Insect Eggs. Pergamon Press, Oxford, UK.
Isaka, Y. and Sato, T., 2014. Was species diversification in Tenthredinoidea (Hymenoptera: Symphyta) related to the origin and diversification of angiosperms? Can. Entomol. 147, 443–458.
Jervis, M. and Vilhelmsen, L., 2000. Mouthpart evolution in adults of the basal, 'symphytan', hymenopteran lineages. Biol. J. Linn. Soc. 70, 121–146.
Jouault, C., Oyama, N., Álvarez-Parra, S., Huang, D.Y., Perrichot, V., Condamine, F.L. and Legendre, F., 2025. The radiation of Hymenoptera illuminated by Bayesian inferences from the fossil record. Curr. Biol. 35, 2164–2174.e4.
Kembel, S.W., Cowan, P.D., Helmus, M.R., Cornwell, W.K., Morlon, H., Ackerly, D.D., Blomberg, S.P. and Webb, C.O., 2010. Picante: R tools for integrating phylogenies and ecology. Bioinformatics 26, 1463–1464.
Krasilov, V.A. and Rasnitsyn, A.P., 1982. A unique find: pollen in the intestine of early Cretaceous sawflies. Paleontol. Zh. 4, 83–96.
Krassilov, V., Tekleva, M., Meyer-Melikyan, N. and Rasnitsyn, A., 2003. New pollen morphotype from gut compression of a Cretaceous insect, and its bearing on palynomorphological evolution and palaeoecology. Cretac. Res. 24, 149–156.
Krogmann, L., Engel, M.S., Bechly, G. and Nel, A., 2012. Lower Cretaceous origin of long-distance mate finding behaviour in Hymenoptera (Insecta). J. Syst. Palaeontol. 11, 83–89.
Labandeira, C.C., 2014. Why did terrestrial insect diversity not increase during the angiosperm radiation? Mid-Mesozoic, plant-associated insect lineages harbor clues. In: Pontarotti, P. (Ed.), Evolutionary Biology: Genome Evolution, Speciation, Coevolution and Origin of Life. Springer, Cham, Switzerland, pp. 261–299.
Lehtonen, S., Silvestro, D., Karger, D.N., Scotese, C., Tuomisto, H., Kessler, M., Peña, C., Wahlberg, N. and Antonelli, A., 2017. Environmentally driven extinction and opportunistic origination explain fern diversification patterns. Sci. Rep. 7, 4831.
Leppänen, S.A., Altenhofer, E., Liston, A.D. and Nyman, T., 2012. Phylogenetics and evolution of host-plant use in leaf-mining sawflies (Hymenoptera: Tenthredinidae: Heterarthrinae). Mol. Phylogenet. Evol. 64, 331–341.
Lewis, P.O., 2001. A likelihood approach to estimating phylogeny from discrete morphological character data. Syst. Biol. 50, 913–925.
Malagón-Aldana, L.A., Smith, D.R., Shinohara, A. and Vilhelmsen, L., 2021. From *Arge* to *Zenarge*: adult morphology and phylogenetics of argid sawflies (Hymenoptera: Argidae). Zool. J. Linnean Soc. 193, 880–938.
Malagón-Aldana, L.A., Jensen, A.R., Smith, D.R., Shinohara, A. and Vilhelmsen, L., 2022. Sawflies out of Gondwana: phylogenetics and biogeography of Argidae (Hymenoptera). Syst. Entomol. 47, 231–258.
Malm, T. and Nyman, T., 2015. Phylogeny of the symphytan grade of Hymenoptera: new pieces into the old jigsaw(fly) puzzle. Cladistics 31, 1–17.
Nel, A., Petrulevičius, J.F. and Henrotay, M., 2004. New Early Jurassic sawflies from Luxembourg: the oldest record of Tenthredinoidea (Hymenoptera: "Symphyta"). Acta Palaeontol. Pol. 49, 283–288.
Niu, G.Y., Budak, M., Korkmaz, E.M., Doğan, Ö., Nel, A., Wan, S.Y., Cai, C.Y., Jouault, C., Li, M. and Wei, M.C., 2022. Phylogenomic analyses of the Tenthredinoidea support the familial rank of Athaliidae (Insecta, Tenthredinoidea). Insects 13, 858.
Nixon, K.C., 1996. Paleobotany in cladistics and cladistics in paleobotany: Enlightenment and uncertainty. Rev. Palaeobot. Palynol. 90, 361–373.
Nixon, K.C., 2002. WinClada, Version 1.00.08. Published by the author, Ithaca, NY, USA.
Nyman, T., Farrell, B.D., Zinovjev, A.G. and Vikberg, V., 2006. Larval habits, host-plant associations, and speciation in nematine sawflies (Hymenoptera: Tenthredinidae). Evolution 60, 1622–1637.
Nyman, T., Onstein, R.E., Silvestro, D., Wutke, S., Taeger, A., Wahlberg, N., Blank, S.M. and Malm, T., 2019. The early wasp plucks the flower: disparate extant diversity of sawfly superfamilies (Hymenoptera: 'Symphyta') may reflect asynchronous switching to angiosperm hosts. Biol. J. Linn. Soc. 128, 1–19.
Paradis, E. and Schliep, K., 2019. ape 5.0: an environment for modern phylogenetics and evolutionary analyses in R. Bioinformatics 35, 526–528.
Pattinson, D.J., Thompson, R.S., Piotrowski, A.K. and Asher, R.J., 2015. Phylogeny, paleontology, and primates: do incomplete fossils bias the tree of life? Syst. Biol. 64, 169–186.
Peris, D., Labandeira, C., Barrón, E., Delclòs, X., Rust, J. and Wang, B., 2020. Generalist pollen-feeding beetles during the mid-Cretaceous. iScience 23, 100913.
Quicke, D.L.J., 1997. Parasitic Wasps. Chapman and Hall, London.
R Core Team, 2023. R: A Language and Environment for Statistical Computing. R Foundation for Statistical Computing, Vienna.
Rasnitsyn, A.P., 1969. Origin and evolution of lower Hymenoptera. Tr. Paleontol. Inst. Acad. Nauk SSSR 123, 1–196 (in Russian).
Rasnitsyn, A.P., 1980. Origin and evolution of Hymenoptera. Tr. Paleontol. Inst. Acad. Nauk SSSR 174, 1–192.
Rasnitsyn, A.P., 1988. An outline of evolution of the hymenopterous insects (order Vespida). Orient. Insects 22, 115–145.
Rasnitsyn, A.P., 1996. Conceptual issues in phylogeny, taxonomy, and nomenclature. Contrib. Zool. 66, 3–41.
Rasnitsyn, A.P. and Manukyan, A.R., 2023. A new species of the family Electrotomidae (Hymenoptera, Symphyta, Tenthredinoidea) from the Baltic amber. Paleontol. J. 57, 541–546.

Rasnitsyn, A.P. and Müller, P., 2023. Identity of the insect larva described by Zippel et al. (2022) in the mid-Cretaceous Burmese (Kachin) amber (Hymenoptera, Tenthredinoidea, Blasticotomidae = Xyelotomidae syn. nov.). Palaeoentomology 6, 13–16.
Rasnitsyn, A.P., Jarzembowski, E.A. and Ross, A.J., 1998. Wasps (Insecta: Vespida = Hymenoptera) from the Purbeck and Wealden (Lower Cretaceous) of southern England and their biostratigraphical and palaeoenvironmental significance. Cretac. Res. 19, 329–391.
Ren, D., 1998. Flower-associated Brachycera flies as fossil evidence for Jurassic angiosperm origins. Science 280, 85–88.
Ren, D., Shih, C.K., Gao, T.P., Wang, Y.J. and Yao, Y.Z., 2019. Rhythms of Insect Evolution – Evidence From the Jurassic and Cretaceous in northern Chiba. Wiley Blackwell, Hoboken, NJ.
Revell, L.J., 2024. phytools 2.0: an updated R ecosystem for phylogenetic comparative methods (and other things). PeerJ 12, e16505.
Richards, O.W., 1985. Hymenoptera, Introduction and Key to Families (X.F. Zhao, Trans.). Science Press, Beijing, China. (Original work published 1977).
Rodriguez, J., Frese, M., Dettmann, M., Chavoshi-Jolfaei, M. and Macdonald, J., 2024. A new exceptionally preserved sawfly fossil (Hymenoptera: Pergidae) and an evaluation of its utility for divergence time estimation and biogeography. Syst. Entomol. 50, 237–251.
Romero-Lebrón, E., Robledo, J.M., Delclòs, X., Petrulevičius, J.F. and Gleiser, R.M., 2022. Endophytic insect oviposition traces in deep time. Palaeogeogr. Palaeocl. 590, 110855.
Ronquist, F., Rasnitsyn, A.P., Roy, A., Eriksson, K. and Lindgren, M., 1999. Phylogeny of the Hymenoptera: a cladistic reanalysis of Rasnitsyn's (1988) data. Zool. Scr. 28, 13–50.
Ronquist, F., Klopfstein, S., Vilhelmsen, L., Schulmeister, S., Murray, D.L. and Rasnitsyn, A.P., 2012. A total-evidence approach to dating with fossils, applied to the early radiation of the Hymenoptera. Syst. Biol. 61, 973–999.
Rueden, C.T., Schindelin, J., Hiner, M.C., DeZonia, B.E., Walter, A.E., Arena, E.T. and Eliceiri, K.W., 2017. ImageJ2: ImageJ for the next generation of scientific image data. BMC Bioinformatics 18, 529.
Schulmeister, S., 2003. Review of morphological evidence on the phylogeny of basal Hymenoptera (Insecta), with a discussion of the ordering of characters. Biol. J. Linn. Soc. 9, 209–243.
Silvestro, D., Salamin, N., Antonelli, A. and Meyer, X., 2019. Improved estimation of macroevolutionary rates from fossil data using a Bayesian framework. Paleobiology 45, 546–570.
Spencer, M.R. and Wilberg, E.W., 2013. Efficacy or convenience? Model-based approaches to phylogeny estimation using morphological data. Cladistics 29, 663–671.
Sun, G., Dilcher, D.L., Zheng, S.L. and Zhou, Z.K., 1998. In search of the first flower: A Jurassic angiosperm, *Archaefructus*, from northeast China. Science 282, 1692–1695.
Sun, G., Ji, Q., Dilcher, D.L., Zheng, S.L., Nixon, K.C. and Wang, X.F., 2002. Archaefructaceae, a new basal angiosperm family. Science 296, 899–904.
Sun, C.H., Rasnitsyn, A.P., Wedmann, S., Zhuang, J.L., Shih, C.K., Ren, D. and Gao, T.P., 2024. Revisions, new taxa, and venation transformations of the sawfly family Blasticotomidae *sensu lato* (Hymenoptera: Tenthredinoidea) highlight the evolution of the basal Hymenoptera. Zool. J. Linnean Soc. 202, zlae113.
Taeger, A., Liston, A.D., Prous, M., Groll, E.K., Gehroldt, T. and Blank, S.M., 2018. ECatSym – Electronic world catalog of Symphyta (Insecta, Hymenoptera). Available at: https://www.sdei.de/ecatsym/.
Vilhelmsen, L., 2000. The ovipositor apparatus of basal Hymenoptera (Insecta): phylogenetic implications and functional morphology. Zool. Scr. 29, 319–345.
Vilhelmsen, L., 2001. Phylogeny and classification of the extant basal lineages of the Hymenoptera (Insecta). Zool. J. Linnean Soc. 131, 393–442.
Vilhelmsen, L., 2015. Morphological phylogenetics of the Tenthredinidae (Insecta: Hymenoptera). Invertebr. Syst. 29, 164–190.
Vilhelmsen, L., Perkovsky, E.E. and Jenkins Shaw, J., 2024. Rogue sawflies: Rare late Eocene amber fossils provide new calibration points for dating the evolution of Tenthredinoidea (Insecta: Hymenoptera). J. Syst. Palaeontol. 22, 2348774.
Walker, F.M., Dunhill, A.M. and Benton, M.J., 2019. Variable preservation potential and richness in the fossil record of vertebrates. Palaeontology 63, 313–329.
Wang, M., Rasnitsyn, A.P. and Ren, D., 2013. A new sawfly fossil from the Lower Cretaceous of China elucidates the antennal evolution in lower Hymenoptera (Pamphilioidea: Praesiricidae: Archoxyelydinae subfam. n.). Syst. Entomol. 38, 577–584.
Wang, B., Xu, C.P. and Jarzembowski, E.A., 2022. Ecological radiations of insects in the Mesozoic. Trends Ecol. Evol. 37, 529–540.
Weltz, C.-E. and Vilhelmsen, L., 2014. The saws of sawflies: exploring the morphology of the ovipositor in Tenthredinoidea (Insecta: Hymenoptera), with emphasis on Nematinae. J. Nat. Hist. 48, 133–183.
Woolley, C.H., Bottjer, D.J., Corsetti, F.A. and Smith, N.D., 2024. Quantifying the effects of exceptional fossil preservation on the global availability of phylogenetic data in deep time. PLoS One 19, e0297637.
Wutke, S., Blank, S.M., Boevé, J.-L., Faircloth, B.C., Koch, F., Linnen, C.R., Malm, T., Niu, G.Y., Prous, M., Schiff, N.M., Schmidt, S., Taeger, A., Vilhelmsen, L., Wahlberg, N., Wei, M.C. and Nyman, T., 2024. Phylogenomics and biogeography of sawflies and woodwasps (Hymenoptera, Symphyta). Mol. Phylogenet. Evol. 199, 108144.
Xiao, L.F., Labandeira, C.C., Wu, Y.K., Shih, C.K., Ren, D. and Wang, Y.J., 2024. Middle Jurassic insect mines on gymnosperms provide missing links to early mining evolution. New Phytol. 242, 2803–2816.
Xiao, L.F., Chen, L., Labandeira, C.C., Azevedo-Schmidt, L., Wang, Y.J. and Ren, D., 2025. The modern pattern of insect herbivory predates the advent of angiosperms by 60 My. Proc. Natl. Acad. Sci. USA 122, e2412036122.
Zhang, J.F., 1985. Mesozoic insect fossils. Shandong Land Res. 1, 23–39 (In Chinese).
Zhang, G.Y., 2025. guoyi.run: One-step TNT script for maximum parsimony phylogenetic analysis. Zootaxa 5642, 96–98.
Zhang, C., Stadler, T., Klopfstein, S., Heath, T. and Ronquist, F., 2016. Total-evidence dating under the fossilized birth–death process. Syst. Biol. 65, 228–249.
Zhong, Y.T., Huyskens, M.H., Yin, Q.Z., Wang, Y.Q., Ma, Q. and Xu, Y.G., 2021. High-precision geochronological constraints on the duration of 'Dinosaur Pompeii' and the Yixian Formation. Natl. Sci. Rev. 8, nwab063.
Zhou, Z.H., Wang, Y., Xu, X. and Ren, D., 2017. The Jehol Biota: An exceptional window into Early Cretaceous terrestrial ecosystems. In: Fraser, N.C. and Sues, H.D. (Eds.), Terrestrial Conservation Lagerstätten: Windows into the Evolution of Life on Land. Dunedin Academic Press, Edinburgh, UK, pp. 169–214.

Supporting Information

Additional supporting information may be found online in the Supporting Information section at the end of the article.

Fig. S1. †*Eotenthredo sinensis* gen. et sp. nov., Paratype (CNU-HYM-LB2024002), female.

Fig. S2. †*Eotenthredo sinensis* gen. et sp. nov., Paratype (CNU-HYM-LB2024003p/c), female.

Fig. S3. †*Eotenthredo sinensis* gen. et sp. nov., Paratype (CNU-HYM-LB2024004p/c), female.

Fig. S4. †*Eotenthredo sinensis* gen. et sp. nov., Paratype (CNU-HYM-LB2024005p/c), female.

Fig. S5. †*Eotenthredo sinensis* gen. et sp. nov., Paratype (CNU-HYM-LB2024006p/c), female.

Fig. S6. †*Eotenthredo sinensis* gen. et sp. nov., Paratype (CNU-HYM-LB2024007), female.

Fig. S7. †*Eotenthredo magna* gen. et sp. nov., Paratype (CNU-HYM-LB2024009), female. (a) Habitus. (b) Forewing. (c) Antennae.

Fig. S8. †*Evacuxyela hsiaoae* (CNU-HYM-LB2021033), male.

Fig. S9. †*Dahurotoma* sp.

Fig. S10. †*Paradoxotoma tsaiae* (CNU-HYM-NN2008013), male.

Fig. S11. †*Paradoxotoma tsaiae*.

Fig. S12. †*Synaptotoma limi* (CNU-HYM-NN2008012), female.

Fig. S13. †*Apertoma macroclada* (a, d, g) CNU-HYM-NN2024019. (b, e, h), CNU-HYM-NN2024020. (c, f, i) CNU-HYM-NN2024021.

Fig. S14. †*Apertoma macroclada* (a) habitus, ventral view, CNU-HYM-NN2024022c. (b) habitus, dorsal view, CNU-HYM-NN2024022p. (c) habitus, ventral view, CNU-HYM-NN2024023. (d) dorsal view, CNU-HYM-NN2024024. (e) metathorax under alcohol. (f) antennae under alcohol. (g) medioventral mesopleuron. (h) mesothorax under alcohol. Red arrows point to the cenchrus; blue arrows point to the possible lateral grooves. Scale bars: 1 mm in (a–d); 0.5 mm in (e–h). Abbreviations: mc = mesoscutellum, mps = mesoprescutum.

Fig. S15. †*Liberitoma* sp.

Fig. S16. †*Liberitoma* sp.

Fig. S17. †*Xyelocerus* sp.

Fig. S18. Habituses with the corresponding mesothoraxes.

Fig. S19. Habituses with the corresponding mesothoraxes.

Fig. S20. Reference tree used to assess the placement of †*Eotenthredo*.

Fig. S21. Results of MP analysis under EW (seed = 10, CI = 0.58, RI = 0.83, length = 117 steps).

Fig. S22. Results of MP analysis under IW (K = 12, seed = 9, CI = 0.58, RI = 0.83, length = 117 steps).

Table S1. Catalogue of Tenthredinoidea.

Table S2. Detailed information regarding species names, sources and specimen numbers of both fossil and extant specimens examined in this study.

Table S3. Ratios relating to the mesothorax scutum.

Table S4. Ratios relating to the antennae.

Data S1. Descriptions of morphological characters and character states with discussion of character state distributions.

Data S2. Scripts and data for phylogenetic analyses and R-based visualization.